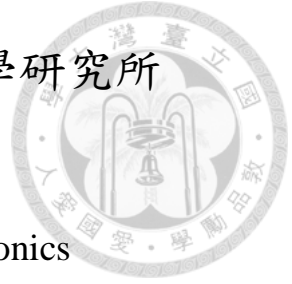


國立臺灣大學電機資訊學院光電工程學研究所

碩士論文

Graduate Institute of Photonics and Optoelectronics  
College of Electrical Engineering and Computer Science  
National Taiwan University  
Master Thesis



氧化銦鎵鋅薄膜電晶體生物感測器應用於蛋白質與配  
體之動態反應分析

Transient Analysis of Protein-Ligand Kinetic Reactions  
Using an IGZO Thin Film Transistor Biosensor

周浚和

Chun-Ho Chou

指導教授：黃建璋 博士

Advisor: Jian-Jang Huang, Ph.D.

中華民國 108 年 8 月

August 2019

國立臺灣大學碩士學位論文  
口試委員會審定書

氧化銦鎵鋅薄膜電晶體生物感測器應用於  
蛋白質與配體之動態反應分析  
Transient Analysis of Protein-Ligand Kinetic  
Reactions Using an IGZO Thin Film Transistor  
Biosensor

本論文係周浚和君（學號 R06941007）在國立臺灣大學  
光電工程學研究所完成之碩士學位論文，於民國 108 年 7 月  
24 日承下列考試委員審查通過及口試及格，特此證明

口試委員：

黃建璋

（指導教授）

林致廷

李翔傑

黃念祖

賴韋志

所長

林恭如

## 致謝



無數的期待、無數的憧憬、無數的仰望、無數的悸動交織而成，我親自將它們一針一線編織成名為歲月的大衣，許多色彩的點綴著實美艷動人。兩年的碩士生涯很幸運能夠在臺大渡過，特別是能夠加入我的指導教授—黃建璋老師的實驗室。

在這漫漫的求學之旅中，很感謝老師的悉心指導，不僅對於我的研究方向提供堅實的意見，教導了我研究的方法與精神，也全力支持我想嘗試的方向；除此之外，老師也向我們分享了許多生活哲理與未來待人處事的絕門。其中，電梯哲學更是最印象深刻也認為很有價值的知識寶藏，「如何恰當表達自己的想法」我認為是在黃老師實驗室以外很難獲得鍛鍊的技巧。

謝謝我親愛的博舜學長，帶領我進入度日如年的製程實驗室，適時給予我意見幫助我實踐「做出元件」的里程碑。我們一同在深夜的量測時光雖然苦悶，以絕望的呼喊結束每一個夜晚，回想起來也是苦盡甘來，我們努力奮鬥換來了今天的成果。永燦、岱頡、Kuntal 學長，謝謝你們分享生活中的精彩與人生觀。

思瑜同學，謝謝你在我最艱困的時候陪伴我並給予我建議，除了實驗與課業之外也提供了許多想法，讓我這兩年完成的碩士生涯更加充實，甚至更成熟、更堅強，賦予我另一個全新角度看待與詮釋人生。

我的同學們：思瑜、約廷、妍葶，從步入 312 的第一天就開始鬥嘴，話雖如此，大家在該正經的時候依舊能鼎力相助，發揮各位深藏的才能，做製程的意見、選課的消息、考試的技巧、寫作業的捷徑、美食的推薦、旅遊的安排、購物的慾望，彼此間交流了許多，謝謝你們給我如此美好的回憶。

我薄膜電晶體生醫量測組的學弟：耀軒、錦春，謝謝你們對於我展現粗淺絕活時給予我支持與肯定，並且協助我完成艱難的量測，一直被我指使買雜物、做流道、蒐集資料，現在終於可以換你們指使別人了。另外，孟諭學弟與靜好、季璇學妹，謝謝你們這一年的幫助與帶給苦悶實驗室的歡笑。

最後要感謝我的爸爸與媽媽，隨時展開雙臂歡迎我回到避風港，即使我忙得焦頭爛額也不忘提醒我照顧好自己，從不給我學習與成長的壓力，讓我擁有最堅實的後盾，無後顧之憂完成我的碩士學位。

## 中文摘要



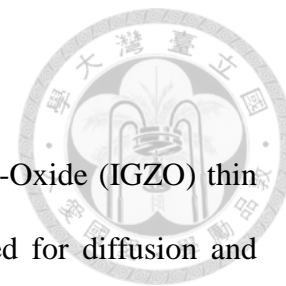
這篇論文介紹以氧化銦鎵鋅薄膜電晶體與感測金屬電極組成之生物感測器偵測生物分子擴散與混合狀態並探討蛋白質與配體之動態反應，此研究分兩部分：

第一部分，分析生物素與鏈親和素的混合情況，我們採用薄膜電晶體生物感測器外接 Y 型微流道。此外，使用聚二甲基矽氧烷來密封微流道系統以避免待測溶液蒸發。接著分別量測生物素與鏈親和素的電流訊號，定義待測物的擴散時間。進行一系列同時與時間差的混合實驗。藉觀察即時的電流變化，分析待測物在流道中的混合狀況。最後我們使用牛血清白蛋白作為對照組，驗證薄膜電晶體生物感測器之非特異性結合情況。

第二部分，以溶菌酶及其適體三乙醯殼三糖作為動態反應分析標的物，改使用直線型微流道作為感測平台。溶菌酶以及三乙醯殼三糖溶液注入微流道感測電流訊號。首先，單獨通入溶菌酶溶液至流道中建立溶菌酶濃度與電流變化關係。將三種濃度比例之溶菌酶以及三乙醯殼三糖混合在離心管中，控制兩者的反應時間；對擷取之電流變化，考量屏蔽效應進行修正後可藉已建立之溶菌酶濃度與電流變化關係將電流變化轉為剩餘溶菌酶濃度。以此，可建立剩餘溶菌酶濃度與反應時間擬合曲線。曲線提供之資訊，可助我們藉化學公式得到反應級數、結合速率常數與分解常數。其中，分解常數之結果為  $39.10 \mu\text{M}$ ，與其他團隊提出之數值十分接近。

關鍵字：薄膜電晶體、生物感測器、微流道、溶菌酶、三乙醯殼三糖、動態反應、反應常數

## ABSTRACT



In this thesis, a biosensor consists of an Indium-Gallium-Zinc-Oxide (IGZO) thin film transistor (TFT) and a gold sensing electrode is demonstrated for diffusion and mixing properties detection of biomolecules. The protein-ligand kinetic reaction is further investigated. The thesis includes two parts.

In the first part, in order to analyze the streptavidin-biotin mixing condition, a Y-type external microfluidic channel is integrated with the TFT biosensor. In addition, the channels are sealed with polydimethylsiloxane to avoid evaporation of the target analyte solutions. The current signals of streptavidin and biotin are measured separately to define the diffusion time. Then, a series of mixing and time delay experiments are conducted. By observing the real-time current change of the TFT biosensor, the mixture condition of the reaction can be analyzed. Finally, bovine serum albumin (BSA) is used for a control experiment to verify the specificity and reliability.

In the second part, kinetic reaction of lysozyme and tri-N-Acetylglucosamine (NAG<sub>3</sub>) are investigated and applied to a TFT biosensor integrated with a linear shape microfluidic channel. First, lysozyme solutions of several concentrations are introduced into the microfluidic channel to construct the relation between lysozyme concentration and drain current variation. Then, three mixing ratios of lysozyme and NAG<sub>3</sub> solution are incubated in the micro-centrifuge for different periods of reaction time. Considering the screen effect, the extracted drain current variations are calibrated by the revision factor and the revised current variations are converted into remained lysozyme concentration by the correlation of current variation and lysozyme concentration. Based on the converted information, the fitting curves of remained lysozyme concentration versus reaction time

are illustrated. The curves provide the information that can be utilized to calculate the partial orders, association rate constant, and dissociation constant by biochemical formulas. It is noteworthy that the derived dissociation constant is 39.10  $\mu\text{M}$ , which is close to the results reported by previous researches.

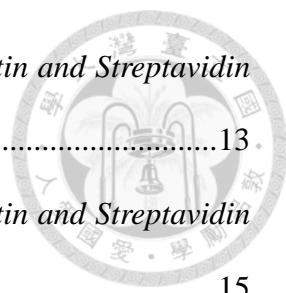
Key words: TFT, biosensor, microfluidic channel, lysozyme, tri-N-acetylglucosamine, kinetic reaction, reaction constant

# CONTENTS



口試委員會審定書 .....	i
致謝 .....	ii
中文摘要 .....	iii
ABSTRACT .....	iv
CONTENTS .....	vi
LIST OF FIGURES .....	viii
LIST OF TABLES .....	xii
<b>Chapter 1 Introduction.....</b>	<b>1</b>
1.1 Overview of Biochemical Detection .....	1
1.2 Introduction of FET-based Biosensors .....	2
1.3 Importance of Biochemical Reaction Kinetics .....	4
1.4 Thesis Outline .....	5
<b>Chapter 2 IGZO-TFT Biosensors for Investigation of Biotin-Protein Interaction .....</b>	<b>6</b>
2.1 Introduction.....	6
2.2 Material and Methods .....	7
2.2.1 <i>Fabrication of IGZO-TFT Biosensors Integrated with Y-type Microfluidic Channels</i> .....	7
2.2.2 <i>Measurement and experiment flow</i> .....	10
2.3 Results and Discussion .....	12
2.3.1 <i>Confirmation of diffusion dominant or flow dominant</i> .....	12

2.3.2	<i>Transient drain current responses by applying Biotin and Streptavidin separately</i> .....	13
2.3.3	<i>Transient drain current responses by applying Biotin and Streptavidin mixture</i> .....	15
2.3.4	<i>Delay experiment of Biotin and Streptavidin reaction in the microfluidic channel</i> .....	17
2.3.5	<i>BSA control experiment</i> .....	21
2.4	Summary .....	24
<b>Chapter 3 IGZO-TFT Biosensors for Investigation of Protein-Ligand Kinetics.....25</b>		
3.1	Introduction.....	25
3.2	Material and Methods .....	26
3.2.1	<i>Introduction of lysozyme and tri-N-acetylglucosamine</i> .....	26
3.2.2	<i>Measurement and experiment flow</i> .....	27
3.3	Results and Discussions.....	29
3.3.1	<i>Real-time analysis of lysozyme and tri-N-acetylglucosamine</i> .....	29
3.3.2	<i>Detection of lysozyme and tri-N-acetylglucosamine kinetic reaction</i> .....	33
3.3.3	<i>Biochemical constants analysis</i> .....	38
3.4	Summary.....	41
<b>Chapter 4 Conclusions.....43</b>		
<b>REFERENCE .....45</b>		



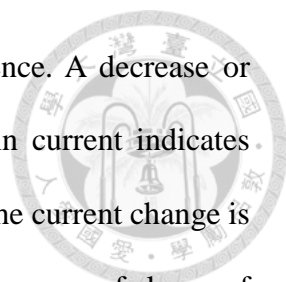


# LIST OF FIGURES



Fig. 1.1	Techniques for biochemical detection. (a) Surface plasma resonance (SPR) (b) Enzyme-linked immunosorbent assay (ELISA) .....	2
Fig. 1.2	(a) Optical image of an FET chip and (b) schematic diagram of the multianalyte FET biosensor for detection of multiple tumor markers. ....	3
Fig. 1.3	TFT-based biosensor structure immobilized with anti-H5N1 antibodies and attached with negatively charged AI H5N1 virus .....	3
Fig. 2.1	The cross section of a staggered and double-gated IGZO-TFT.....	8
Fig. 2.2	Fabrication process of the PDMS replica. ....	9
Fig. 2.3	PDMS bonding treatment flow. ....	10
Fig. 2.4	Microscope up-view of TFT and the microfluidic channel and schematic of the reusable TFT biosensor. The TFT and a microfluidic channel chip were fabricated separately and then connected together by wire bonding. ....	10
Fig. 2.5	Experiment setup for detecting target analytes.....	11
Fig. 2.6	Illustration of the target analyte charge sensing of the TFT biosensor.....	12
Fig. 2.7	Drain current responses of 0.4mM biotin. PBS was applied at t=0 while biotin at t =60 seconds .....	14
Fig. 2.8	Drain current responses of 1.67 $\mu$ M streptavidin. PBS was applied at t=0 while streptavidin at t =60 seconds.....	15
Fig. 2.9	Scenarios of drain current responses when the biotin and streptavidin are applied to the microfluidic channel .....	16
Fig. 2.10	Drain current responses of biotin and streptavidin interactions in the	

	microfluidic channel .....	17
Fig. 2.11	Illustration of the current response scenarios of the streptavidin delay experiment. Biotin solution was introduced in inlet 1 at $t= 60$ s and streptavidin solution was introduced in inlet 2 at $t= 660$ s .....	19
Fig. 2.12	Current response of the streptavidin delay experiment. PBS, biotin and streptavidin were introduced at $t=0, 60$ and $660$ seconds .....	19
Fig. 2.13	Illustration of the current response scenarios for the biotin delay experiment .....	20
Fig. 2.14	Drain current response of the biotin delay experiment. PBS, streptavidin and biotin were introduced at $t=0, 60$ and $660$ seconds .....	21
Fig. 2.15	Transient response of drain current with PBS prefilled at $t=0$ and $0.4\text{mM}$ BSA injected at $t=60$ seconds .....	23
Fig. 2.16	Scenarios of possible BSA-streptavidin interactions once the analytes reach ROI .....	23
Fig. 2.17	Current response of BSA delay experiment. Streptavidin solution was introduced in inlet 1 at $t= 60$ s, and BSA solution was introduced in inlet 2 at $t=660\text{s}$ .....	24
Fig. 3.1	Schematic of the IGZO-TFT biosensor with a linear-shaped microfluidic channel .....	29
Fig. 3.2	Experimental flow which consists of two parts .....	29
Fig. 3.3	Transient drain current properties of a bare TFT chip without and with the injection $0.01\times$ PBS solution .....	31
Fig. 3.4	A schematic drain current profile that illustrates physical events during biomaterial diffusion in the microfluidic channel. When the solution is	



injected at  $t = 200$  s, we first observe injection turbulence. A decrease or increase (depending on species in the solution) of drain current indicates capture of biomaterials by the cross linkers in the ROI. The current change is determined by the slope changes, as compared with the average of slopes of 20 points of earlier time.....31

Fig. 3.5 Transient drain currents for lysozyme solutions of different concentrations.....32

Fig. 3.6 Correlation of drain current change and lysozyme concentration. The equation of the fitting curve is shown in the plot. ....33

Fig. 3.7 Transient TFT drain currents for mixtures of (a) 1 mM lysozyme and 2.5 mM NAG<sub>3</sub>, (b) 2.5 mM lysozyme and 2.5 mM NAG<sub>3</sub>, and (c) 2.5 mM lysozyme and 1 mM NAG<sub>3</sub>. They were all reacted for 1.5 hrs before dispersing to the inlet of microfluidic channel. There are two upward turning points in the curves, one at around 500s and the other at around 850s. The first one corresponds to the arrival of lysozyme while the second of lysozyme-NAG<sub>3</sub> complex.....35

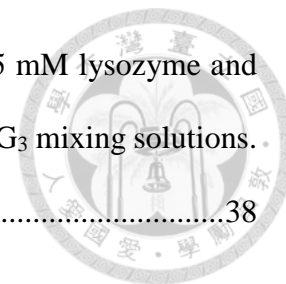
Fig. 3.8 Illustration of molecule capture process of (a) Lysozyme solution (b) lysozyme + NAG<sub>3</sub> solution. The induced drain currents are shown in the right. Note that in addition to the screening effect, with the presence of NAG<sub>3</sub>, the drain current will be increased instead of decreased as opposed to the case of pure lysozyme solution.....36

Fig. 3.9 Drain current changes of the raw and revised responses at different reaction times.....37

Fig. 3.10 Correlation between the remained lysozyme concentration and the reaction

time for (a) 1 mM lysozyme and 2.5 mM NAG<sub>3</sub>, (b) 2.5 mM lysozyme and 2.5 mM NAG<sub>3</sub>, and (c) 2.5 mM lysozyme and 1 mM NAG<sub>3</sub> mixing solutions.

.....38



# LIST OF TABLES



Table 1. The Transmitting of the Dyes of Different Concentrations.....	13
Table 2. Revision Factors of the Mixtures in Our Experiment.....	36
Table 3. Remained Lysozyme, NAG <sub>3</sub> and Complex Concentrations of Three Mixtures, and the Calculated Results of Dissociation Constant, K <sub>d</sub> .....	40
Table 4. Comparisons of Dissociation Constant, K <sub>d</sub> , of Lysozyme–NAG <sub>3</sub> Based on Our Approach and Others Reported in the Literature.....	41



# Chapter 1 Introduction



## 1.1 Overview of Biochemical Detection

The biomedical engineering progresses significantly in the past decade. Especially, the disease diagnostics and drug discovery are the two most attributed issues. Useful information is provided to the biomedical fields by biochemical detection technologies with high accuracy and throughput. Because of early detection and diagnostics, advanced pharmaceutical knowledge, early stage disease prevention and appropriate disease treatment are possible. Several biosensors are developed to reach these goals. A biosensor is an analytical device [1, 2] which can identify the presence of specific analytes [3], their concentrations, and kinetics in a sample by transforming the biological signal into an electrical or optical readout. The device combines a biological recognition element [4] (e.g., antibodies, nucleic acids, enzymes, aptamers) immobilized on a transducer. The ideal properties a biosensor should possess are high accuracy, high sensitivity, high specificity, ease of operation, cost-effective, high throughput, and mass production easily.

Nowadays, traditional methods for biochemical detection such as tumor marker, blood testing, immunological assays, and urinalysis were widely used. However, it is impossible to apply these methods to real time detection and the detection processes are costly, complicated, and time-consuming. Therefore, a simple, accurate, low-cost, and rapid method for detecting and measuring the biomaterials is highly demanded.

Researchers have proposed many advanced techniques for biochemical detection. Among them, surface plasma resonance (SPR) [5], enzyme-linked immunosorbent assay (ELISA) [6] (see Figure 1.1), and western blotting [7] are mature and widely available, but these methods require large and expensive instruments in order to integrate many sensing components for high throughput measurement.

A potential method with properties of accurate, sensitive, high specificity, cost-effective, time-saving, high throughput, label-free, simple, and mass production easily is addressed. The candidate is field-effect transistor (FET)-based biosensor. In this thesis, a thin film transistor (TFT)-based biosensor is demonstrated.

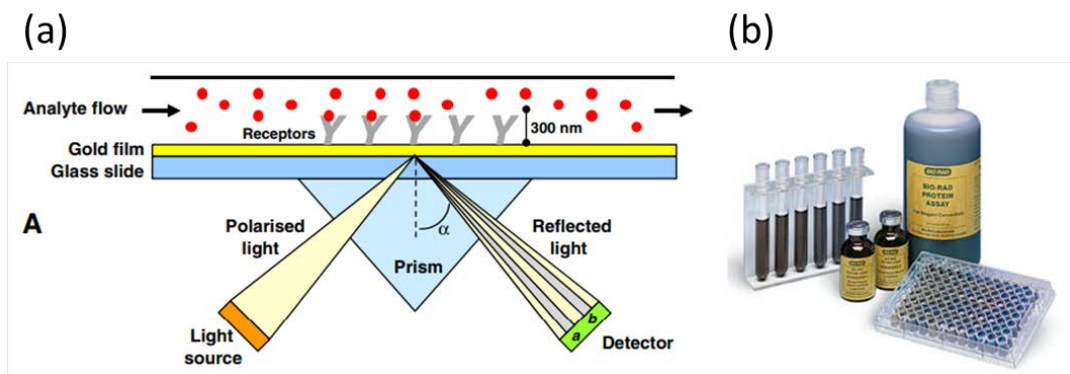
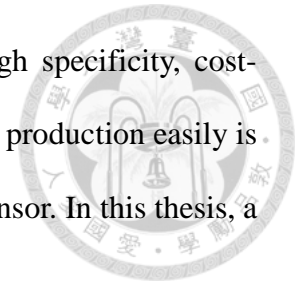


Fig. 1.1 Techniques for biochemical detection. (a) Surface plasma resonance (SPR)  
(b) Enzyme-linked immunosorbent assay (ELISA)

## 1.2 Introduction of FET-based Biosensors

Field effect transistor (FET)-based biosensors are combined with electrochemical solution, microelectronics transistors, and nano-technology. Because of high sensitivity and selectivity, label-free and real-time measurement, FET based biosensors are getting more and more popular. The structure consists of source, drain, gate and a layer that can sense biomolecules such as protein or nucleic acids. When the target solution is introduced to the system, the analytes will attach to the bio-sensitive layer. The attachment makes an electric field formed by the electrical charges which are carried by biomolecules, which leads to the change of carrier density in FET channel layer.

FET-based biosensors are appropriate to various kinds of detection, such as lung cancer diagnosis by observing threshold voltage change as shown in Fig. 1.2 [8].



Moreover, the semiconductor layers, such as ZnO [9], GaN [9], and IGZO [10], are developed and optimized in order to improve sensitivity. The layers play important roles in their applicability to FET biosensors. To be more specific, here take some FET biosensor research for example: enzyme-coated single ZnO nanowire FET biosensor for detection of uric acid [11], indium-tin-oxide thin-film transistors for detecting AI H5N1 through measuring drain current change as shown in Fig. 1.2 [12], and ZnO-TFT-based biosensor for EGFR detection through measuring drain current change [13], indium gallium zinc oxide (IGZO) thin-film transistors (TFTs) for detecting artificial deoxyribonucleic acid [14].

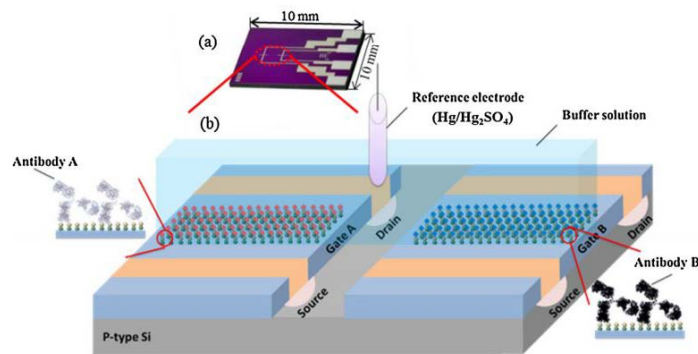


Fig. 1.2 (a) Optical image of an FET chip and (b) schematic diagram of the multianalyte FET biosensor for detection of multiple tumor markers.

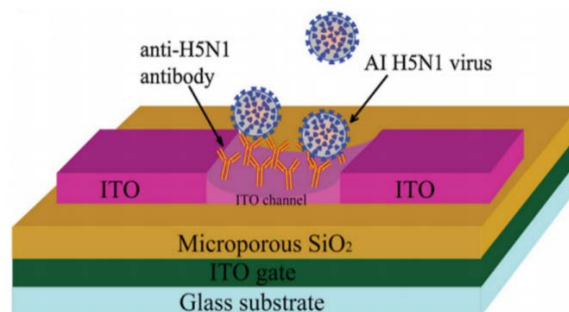


Fig. 1.3 TFT-based biosensor structure immobilized with anti-H5N1 antibodies and attached with negatively charged AI H5N1 virus.



However, the active layer may be damaged by biological solution since oxide semiconductor is sensitive to moisture and oxidant [15]. An extended-gate FET is a robust method to separate electronic devices from the biological solution.

Hence, the IGZO-TFT biosensor with an extended sensing electrode is demonstrated in this research. The extended gold sensing electrode provides an excellent platform for measuring the target biomolecules and also prevents the IGZO-TFT from direct contacting to biological solution effectively.

### **1.3 Importance of Biochemical Reaction Kinetics**

In the biochemical field, analysis of protein-ligand interaction (PLI) raises lots of attentions. Good knowledge of underlying system, i.e., underlying mechanism and kinetic parameters, is indispensable to studies of biological system or applications in drug discovery [16-18]. Because of a drug being effective only when it is bound to its receptor (e.g., proteins) [19], the binding assessment is considered to be important for pharmacological activity. Binding parameters such as the dissociation constant,  $K_d$ , were the key to evaluate the drug efficacy in the past decades. Despite many efficacious drug existing on the basis of parameters, recent studies show that the kinetics of drug receptor binding could be more important than affinity in determining drug efficacy. For some drugs, it is not desirable to attain the equilibrium. The dissociation constant measured from experiments no longer well describe the duration of efficacy of a ligand. Instead, the rate of receptor–ligand association and dissociation, generally reflected by association rate constant,  $k_a$ , and dissociation rate constant,  $k_d$ , are more appropriate. Also, the clinical differentiation and safety may be influenced by the binding kinetics. The optimization of

binding kinetics helps fulfilling the maximization of a drug's therapeutic index and decrease of drug attrition [20-22].



## 1.4 Thesis Outline

Chapter 2 “Detection of the mixing reaction situation of the biomaterials” differentiates biotin, streptavidin, and biotin-streptavidin complex and evaluates the reaction condition of biotin and streptavidin mixing reactions. The fabrication of the TFT biosensor integrated with Y-type microfluidic channel is first introduced. Afterward, diffusion times of both reactant proteins and experiments of the mixing reaction conditions are investigated and discussed. Finally, the non-specific binding situation is verified through the control experiment by applying BSA.

Chapter 3 “Biochemical kinetics investigation” aims at evaluating the binding reaction between the protein and its ligand by extracting the drain current responses. Lysozyme protein and tri-N-acetylglucosamine (NAG<sub>3</sub>) ligand are mixed in three ratios for different periods of reaction time. The different mixing conditions make the drain current response vary. By the analysis of drain current responses, the lysozyme and NAG<sub>3</sub> binding reaction rate constant and dissociation constant are obtained. The result shows good accuracy of the TFT biosensor setup by comparing with the previously reported values.

Chapter 4 “Conclusions” consists of the summary and the importance of the experiments performed in this thesis.

# Chapter 2 IGZO-TFT Biosensors for Investigation of Biotin-Protein Interaction



## 2.1 Introduction

### *Y-type Microfluidic Channel*

In many biomedical applications (e.g. biomedical analysis, drug delivery, chemical synthesis, and enzyme reactions), Y-type Microfluidic Channels, also known as micro-mixers [23, 24], are crucial and have many advantages [25-27]. Less consumption and contamination of bio-samples, as well as the time, are one of the merits.

The materials and fabrication of microfluidic channel have become more important because of the relevance to biology and chemistry during the development of microfluidic system. The characteristics of simple fabrication, optical transparency, and low cost make polymer materials such as PDMS and SU-8 negative photoresist widely used [28, 29].

In this part, PDMS layers is used as the Y-type microfluidic channels. The biological molecules diffuse and interact through the microfluidic channel and the mixture situations are determined by electrical signal and diffusion properties

### *Biotin-Avidin System*

In the past decade, immunocytochemical techniques have a great advancement. For example, the Biotin-Avidin System (BAS), which has the following advantages, is one of them. First, biotin and avidin have an extraordinarily high affinity and specificity between each other. Second, many of the macromolecules can be conjugated to biotin and maintain the original biological activity. Third, the binding reaction is considered irreversible since the dissociation constant of the two is very small. Finally, four binding sites for biotin molecules of each avidin molecule makes it possible to be used to construct an effective

amplification system of biological reaction. BAS are widely used in biological and chemical applications such as tagging or the delivery of molecules, trace antigen, qualitative antibody and quantitative detection [30, 31]. Thus, understanding the mixture condition of the reaction is crucial.

Previous works have presented some optical methods such as fluorescence microscope and enzyme-linked immunosorbent assay (ELISA) [30], but these methods are not real-time measurements. Another study presented a real-time detection method by detecting optical shift of a resonant micro-cavity. In the study, biotinylated BSA was selected as the recognition element and immobilized on the sensing surface followed by the injection of streptavidin, which leads to a shift of the optical resonance wavelength. The shift is due to binding interaction between introduced streptavidin and surface immobilized biotin [32]. Even though the study has preliminary determination ability of the occurrence of biotin and streptavidin binding reaction, a demand on further analyzing the internal mixture interaction in the BAS system still exists.

In this study, we demonstrated an IGZO-TFT biosensor for detecting the mixture situation of biotin and streptavidin. In addition, an analysis and experiment framework was discussed, which is useful on delving into further properties of the BAS reaction. Moreover, bovine serum albumin (BSA) was applied as the control sample and several control experiments were conducted to verify the system specificity and the analysis theory.

## **2.2 Material and Methods**

### **2.2.1 Fabrication of IGZO-TFT Biosensors Integrated with Y-type Microfluidic Channels**

#### *Fabrication of IGZO-TFT*

The cross section of the double-gated IGZO-TFT is shown in Fig. 2.1. A Staggered bottom-gate TFT with the top gate was fabricated on the Corning Eagle 2000 glass substrate. The fabrication started with DC sputtering and reactive ion etching (RIE) molybdenum (Mo) metal as bottom gate. A silicon dioxide (SiO<sub>2</sub>) dielectric layer of 300 nm was deposited by plasma enhanced chemical vapor deposition (PECVD) at 300°C as insulator. Then, 50-nm IGZO (In<sub>2</sub>O<sub>3</sub>:Ga<sub>2</sub>O<sub>3</sub>:ZnO =1:1:1) thin film was formed by RF sputtering at room temperature and etched by HCl wet etching to form the active layer with 100- $\mu$ m channel width and 50- $\mu$ m channel length . The 200-nm Mo source and drain contact layer was deposited by DC sputtering and etched by RIE. A SiO<sub>2</sub> passivation layer was deposited by RF sputtering and followed by RIE etching to prevent the TFT from humidity and oxidation. The top gate with the thickness of 300-nm gold metal was evaporated by E-gun evaporation with lift-off technique. Finally, the fabrication process was finished with post-annealing under oxygen ambient at 270 °C for 30 minutes in the oven tube.

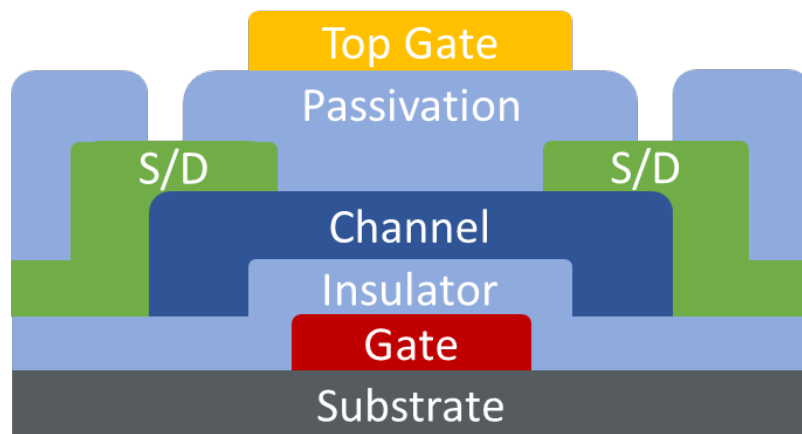
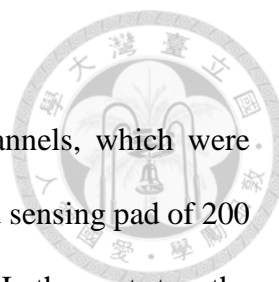


Fig. 2.1 The cross section of a staggered and double-gated IGZO-TFT.



### *Fabrication of Y-type Microfluidic Channels*

The target biomaterials were applied on the microfluidic channels, which were fabricated on a separate glass substrate from the TFT chips. The Au sensing pad of 200 nm was first evaporated on the Corning Eagle 2000 glass substrate. In the next step, the PDMS prepolymer and curing agent (Sylgard 184 silicone elastomer kit, Dow Corning, Midland, MI) were mixed in the weight ratio of 10:1 and stirred well [33]. The PDMS viscous solution was then poured over the Y-shape acrylic patterned mold contained in a circular flat-bottomed polystyrene Petri dish followed by curing at 80 °C for 20 mins. After curing, the PDMS replica of the patterned mold was peeled off the Petri dish and cut into a proper rectangular shape containing microfluidic channels. Fig. 2.2 shows the fabrication process of the PDMS replica.

The PDMS and glass substrate were brought together to form an irreversible seal after treated with oxygen plasma for 6 mins at 70 °C in the UV Ozone [34, 35]. The width and length of the microfluidic channel are 1000 and 10000  $\mu\text{m}$ , respectively. Fig. 2.3 illustrates the PDMS bonding treatment flow. As illustrated in Fig. 2.4, the top gate contact of the TFT is wire bonded by Au wires to the Au metal pad of the microfluidic channel chip. The Y-type microfluidic channel contains two inlets and one outlet, the region of interest (ROI) was selected at the end of the microfluidic channel.

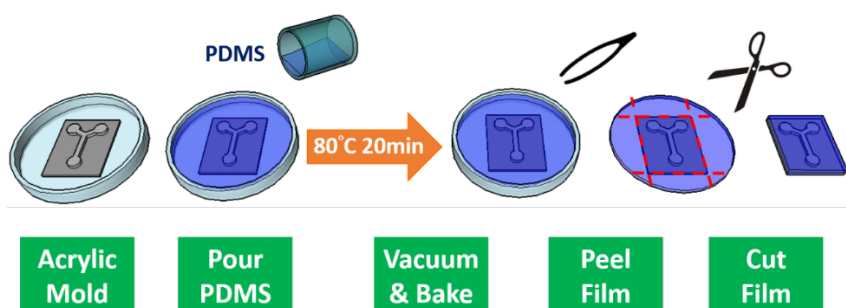


Fig. 2.2 Fabrication process of the PDMS replica.

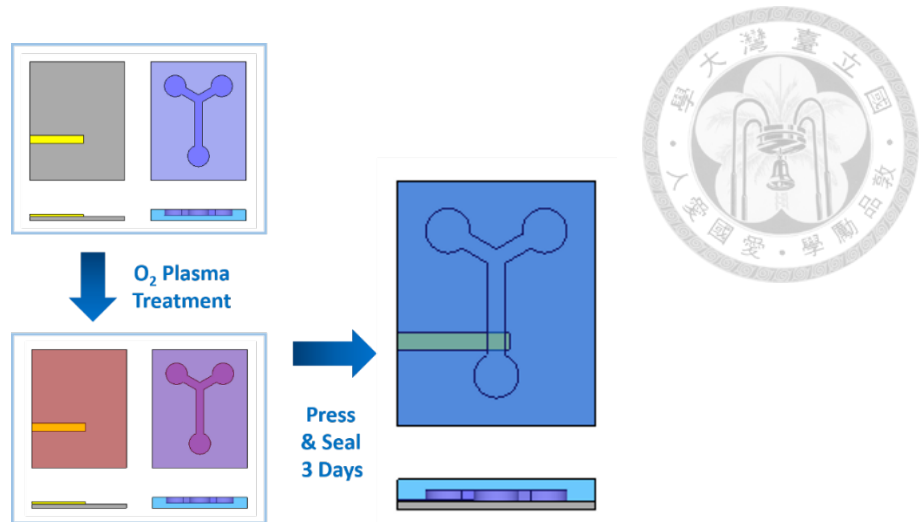


Fig. 2.3 PDMS bonding treatment flow.

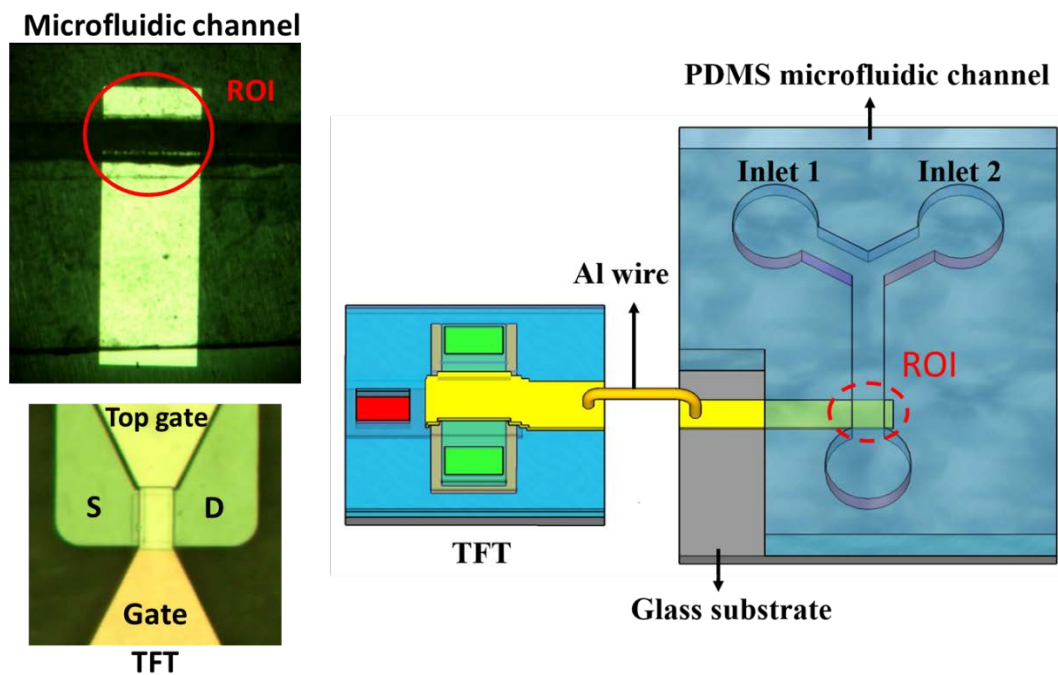


Fig. 2.4 Microscope up-view of TFT and the microfluidic channel and schematic of the reusable TFT biosensor. The TFT and a microfluidic channel chip were fabricated separately and then connected together by wire bonding.

### 2.2.2 Measurement and experiment flow

The experiment setup is shown in Fig. 2.5. The ROI was functionalized with 11-Mercaptoundecanoic acid (11-MUA) cross linker for 2 hours at room temperature and



washed by phosphate buffered saline (PBS). The analytes were introduced into the microfluidic channel by Chemyx Fusion 200 syringe pump.

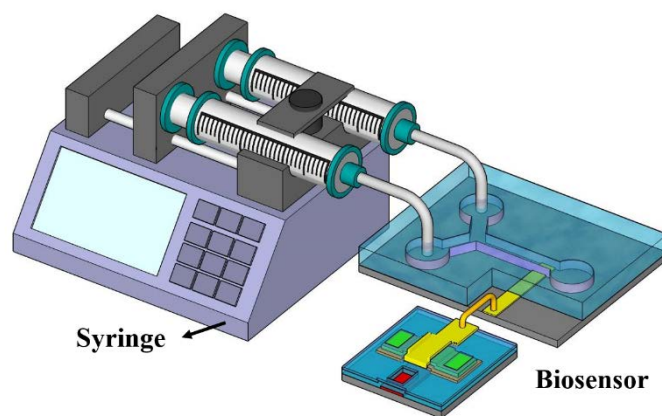


Fig. 2.5 Experiment setup for detecting target analytes

The experiment aims at demonstrating the TFT sensor system as the platform for monitoring real-time biochemical reactions. The target analytes that diffuse through the microfluidic channel and reach the ROI will be captured by the cross linkers. Much proteins and biomaterials carry net charges. As illustrated in Fig. 2.6, additional charges will be induced in the TFT channel layer once the target proteins were sensed on the Au sensing electrode. The amount of drain current change is relevant to the concentration of the analytes.

Using the reaction of biotin and streptavidin as an example, the diffusion behaviors of biotin, streptavidin and biotin-streptavidin complex are characterized. The measurement consists of two steps. The diffusion times of biotin and streptavidin are first benchmarked by injecting the analyte at the inlet and meanwhile monitoring the real-time response of TFT drain current. In the second step, both biotin and streptavidin were applied into one single microfluidic channel chip. Signals of the individual analyte and the reaction complex were examined by the drain current response. Two delay measurements, i.e., one specie is injected 10 mins later than another one, were carried out

to understand the reaction dynamics of the mixture in the microfluidic channel. Finally, a control experiment is conducted. There is no nonspecific binding between bovine serum albumin (BSA) and streptavidin. It can be used to examine the reliability and the specificity of the previous experiments. In the control measurement, biotin is replaced with a 0.4mM BSA solution. The current response of the BSA and streptavidin mixture is compared with that of biotin and streptavidin.

Throughout the experiment, the electrical characteristics were characterized by Agilent 4155C semiconductor parameter analyzer. The TFT was biased at gate-source voltage,  $V_{GS}$ , of 10 V, and drain-source voltage,  $V_{DS}$ , of 5 V. The drain currents were sampled every 10 seconds.

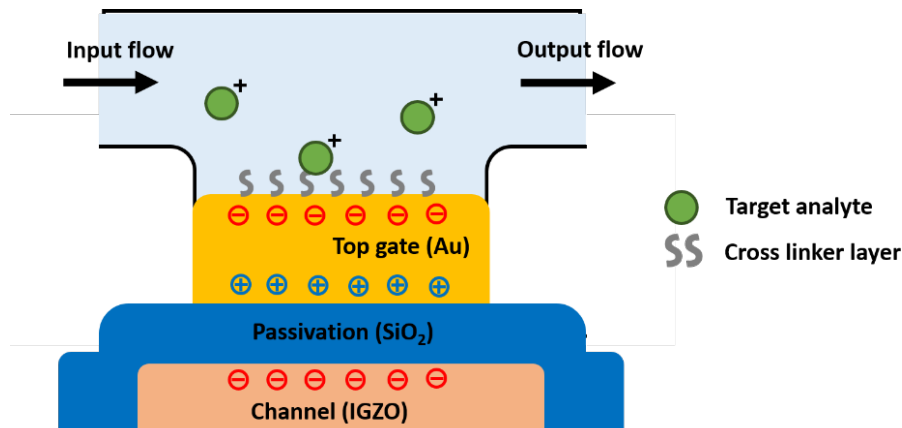


Fig. 2.6 Illustration of the target analyte charge sensing of the TFT biosensor

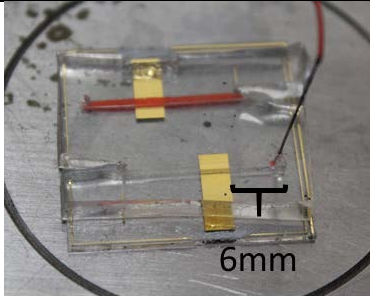
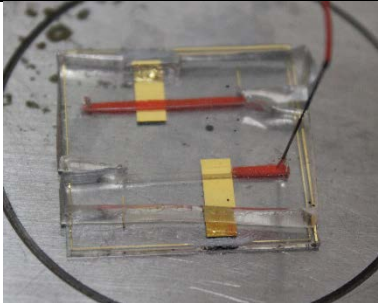
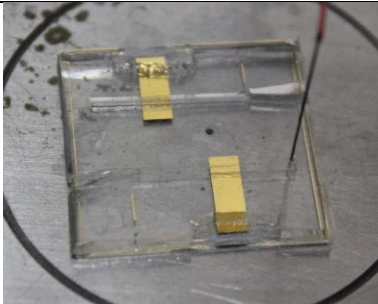
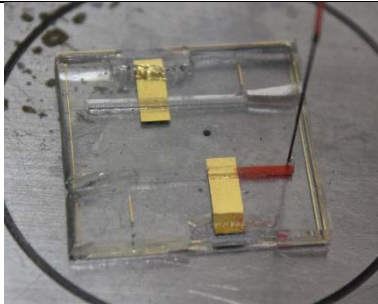
## 2.3 Results and Discussion

### 2.3.1 Confirmation of diffusion dominant or flow dominant

In order to confirm the transmitting of biomolecules is diffusion dominant or flow dominant, the dye was injected into the microfluidic channel at the flow rate of 0.0003

ml/min, which is the same as that of the measurement. The cross-sectional area of the channel is  $1 \text{ mm}^2$  and the distance between the inlet and the electrode is  $6 \text{ mm}$ . If the transmitting mechanism is flow dominant, the flowing time will be  $1200 \text{ s}$ . In Table 1, the durations between the injection and the arrival of dye at electrode are much shorter than  $1200 \text{ s}$ . Therefore, the flow rate is low enough to make the transmitting mechanism being diffusion dominant.

Table 1. The Transmitting of the Dyes of Different Concentrations

Concentration	Start of injection	Arrival at electrode
1	 $t = 0 \text{ s}$	 $t = 200 \text{ s}$
1/4	 $t = 0 \text{ s}$	 $t = 340 \text{ s}$

### 2.3.2 Transient drain current responses by applying Biotin and Streptavidin separately

The streptavidin and biotin diffusion times are first benchmarked. The biotin concentration was selected to be  $0.4 \text{ mM}$  and streptavidin concentration is  $1.67 \mu\text{M}$ . The PBS buffer was prefilled into microfluidic channel at  $t = 0$  second. Biotin solution was then injected  $60$  second later. The drain currents of the TFT are sampled every  $10$  seconds

under  $V_{GS} = 10 \text{ V}$ ,  $V_{DS} = 5 \text{ V}$ . The transient responses of TFT drain current for biotin and streptavidin are shown in Fig. 2.7 and Fig. 2.8. The measurements for each analyte were conducted twice and denoted as Measurement 1 and Measurement 2. The increases of the drain current are the results of the detection of biotin and streptavidin flowing through the ROI and bonded to the cross linker. Since biotin and streptavidin carry net charges, the increase of drain current is associated with the concentration of biomolecules. For biotin, the onset of the drain current was detected at  $t = 210$  seconds for Measurement 1 and  $t = 240$  for Measurement 2. The diffusion time is defined as the duration between the introduction of the target analyte and the onset of drain current increase. Therefore, the diffusion time of biotin in this measurement system is in the range between 150 and 180 seconds. As for streptavidin, the current increases at  $t = 460$  and  $t = 480$  seconds, so the diffusion time of streptavidin is in the range of 400 and 420 seconds.

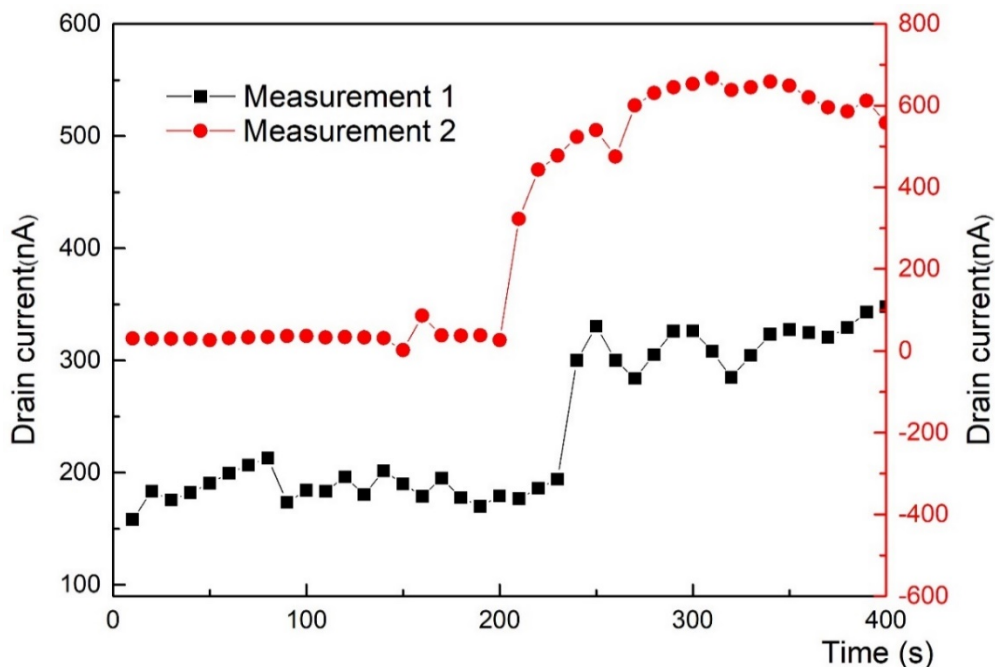


Fig. 2.7 Drain current responses of 0.4mM biotin. PBS was applied at  $t=0$  while biotin at  $t = 60$  seconds

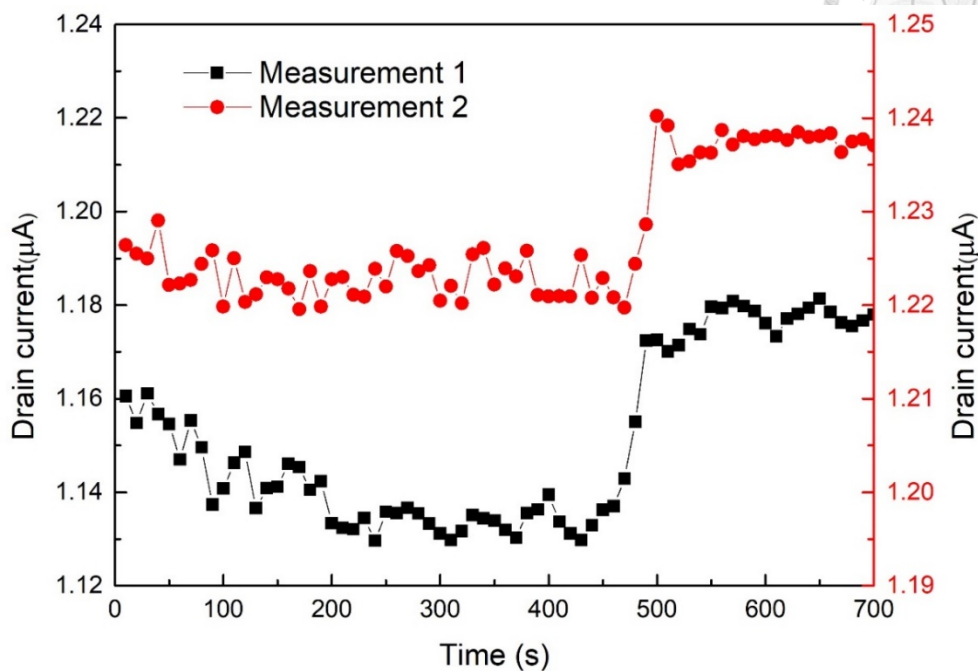
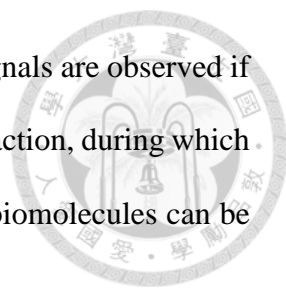


Fig. 2.8 Drain current responses of  $1.67\mu\text{M}$  streptavidin. PBS was applied at  $t=0$  while streptavidin at  $t=60$  seconds

### 2.3.3 Transient drain current responses by applying Biotin and Streptavidin mixture

The analysis of biotin-streptavidin biochemical reactions was next conducted. Before looking into the responses of the mixture, mechanism of biotin and streptavidin interaction in the Y-shaped microfluidic channel is first discussed. The specific diffusion times  $t_1$ ,  $t_2$  and  $t_3$  are defined as the characteristics of biotin, streptavidin, and streptavidin-biotin complex, respectively. There are four possible scenarios as illustrated in Fig. 2.9 when the analytes are injected into inlet 1 and 2 simultaneously. Fig. 2.9(a) denotes the biotin, streptavidin and biotin-streptavidin complex biomolecules reach the ROI in sequence. Three species detected after the reaction is indicated by three obvious current incremental steps. In the second case, when the streptavidin is exhausted during the reaction process, only the biotin and complex signals are detected (see Fig. 2.9(b)). On



the other hand, Fig. 2.9(c) shows only streptavidin and complexes signals are observed if biotin molecules are all consumed. Finally, in the case of complete reaction, during which no biotin and streptavidin are left in the channel, only the complex biomolecules can be detected (see Fig. 2.9(d)).

In the experiment, PBS was introduced at 0 second and streptavidin ( $1.67\mu\text{M}$ ) and biotin ( $0.4\text{mM}$ ) were applied in inlet 1 and inlet 2 (see Fig. 2.4) 60 seconds later, respectively. They may be mixed and react in the microfluidic channel into complexes. The experiment was conducted on two different devices, denoted as measurement 1 and measurement 2. There are two distinct current increment steps in Fig. 2.10. The first one at around  $t = 220$  seconds (diffusion time of  $\sim 160$  seconds) corresponds to the signal of biotin and the second response is at  $t = 740$  seconds, which is longer than the diffusion time of streptavidin in Fig. 2.8. The increase at  $t = 740$  seconds is attributed to the biotin-streptavidin complexes for the  $1.67\mu\text{M}$  of streptavidin being all consumed in the reaction of biotin and streptavidin. The results in Fig. 2.10 correspond to the assumption in Fig. 2.9(b).

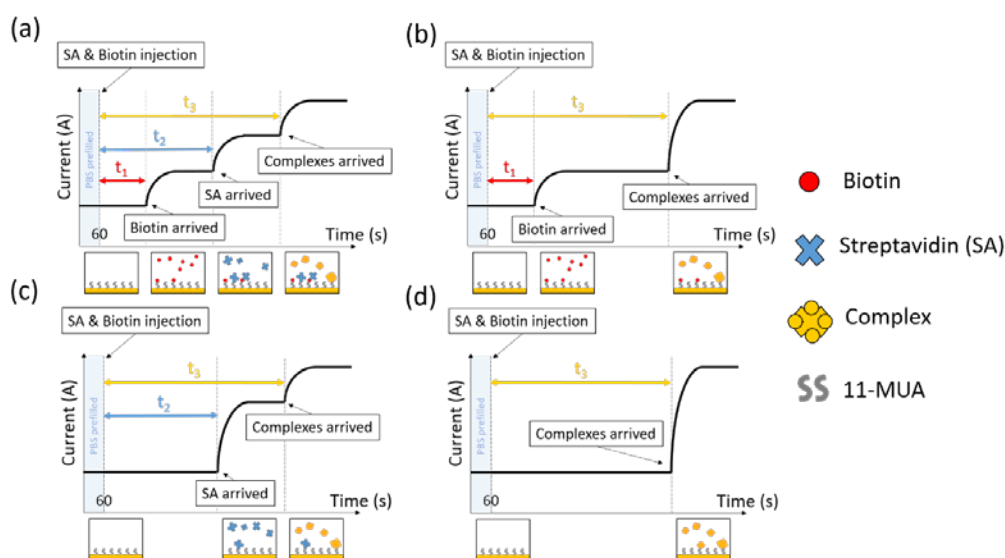


Fig. 2.9 Scenarios of drain current responses when the biotin and streptavidin are applied to the microfluidic channel

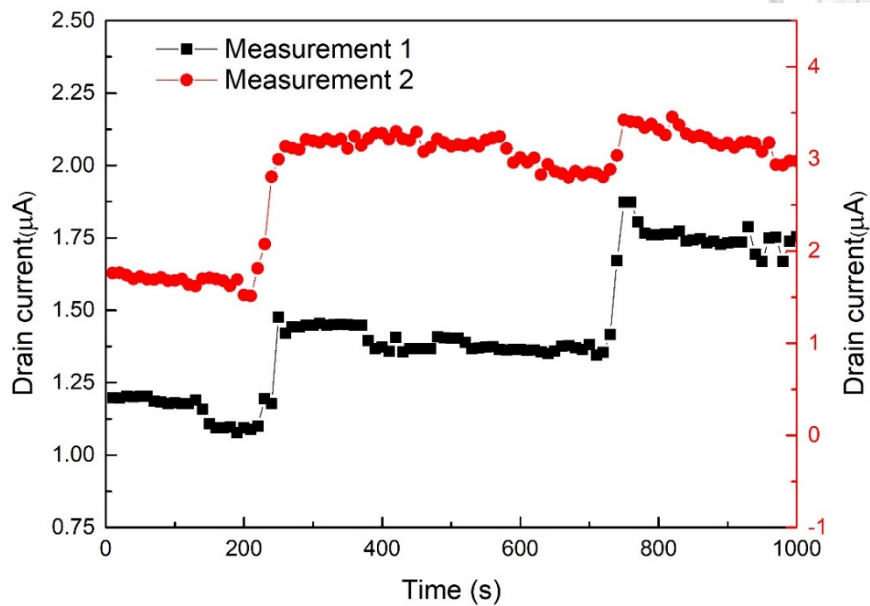
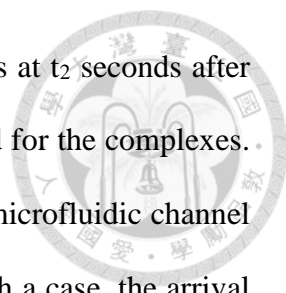


Fig. 2.10 Drain current responses of biotin and streptavidin interactions in the microfluidic channel

### 2.3.4 Delay experiment of Biotin and Streptavidin reaction in the microfluidic channel

In order to further understand the biochemical reaction of biotin and streptavidin, the experiments of either streptavidin or biotin being delayed to be injected into the microfluidic channel was designed. In the first case, defined as streptavidin delay experiment, after PBS pre-filled at  $t=0$ , biotin and PBS were introduced into inlet 1 and 2 at  $t=60$  seconds, respectively. At 660 seconds, the injection of PBS solution was replaced with streptavidin solution.

In Fig. 2.11, possible scenarios of streptavidin delay experiment is shown. For the first case in Fig. 2.11(a), the condition that streptavidin can't react with biotin is assumed. It means that even though they meet with each other in the channel, there is no reaction



occurs and no complex production. Thus, the drain current increases at  $t_2$  seconds after the injection of streptavidin and no third current increase is observed for the complexes. For the second scenario, the biotin molecules are distributed in the microfluidic channel and thus all of streptavidin molecules are reacted with biotin. In such a case, the arrival signal of the complexes will be observed, while that of streptavidin will be missing (see Fig. 2.11(b)). For the last scenario as shown in Fig. 2.11(c), only part of the streptavidin molecules bind with biotin. There will be three increase steps in the transient response of drain current.

To verify the reaction when the streptavidin injection is delayed for 10 minutes, the experiment as described above is conducted. Biotin is introduced at  $t=60$  seconds and streptavidin is at  $t=660$  seconds. In Fig. 2.12, the results are shown. The drain current increase at 250 seconds indicates the arrival of biotin at ROI. Whereas, the diffusion signal of streptavidin is barely seen. A current increase at  $t=1320$  seconds suggests the signal of the biotin-streptavidin complexes. The experiment coincides with the scenario described in Fig. 2.11(b), which indicates the reaction of biotin and streptavidin in the microfluidic channel.



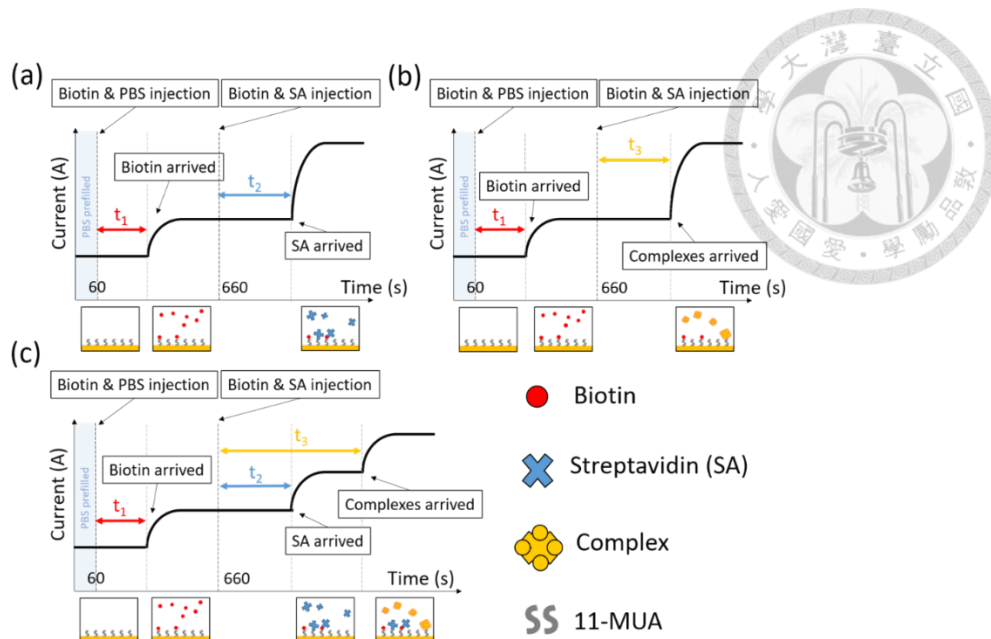


Fig. 2.11 Illustration of the current response scenarios of the streptavidin delay experiment. Biotin solution was introduced in inlet 1 at  $t= 60$  s and streptavidin solution was introduced in inlet 2 at  $t= 660$  s

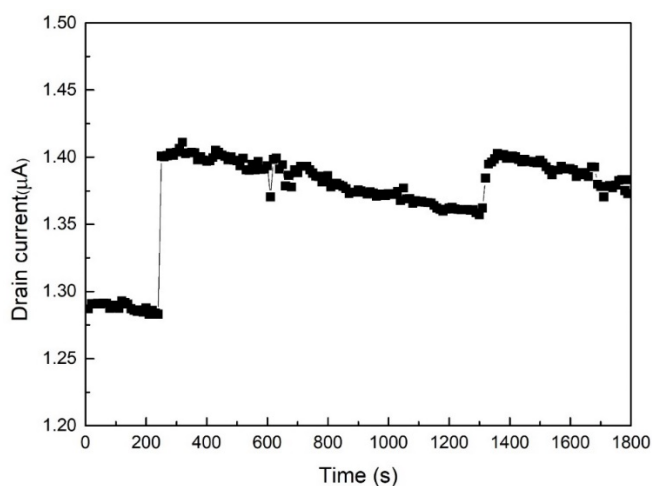


Fig. 2.12 Current response of the streptavidin delay experiment. PBS, biotin and streptavidin were introduced at  $t =0, 60$  and  $660$  seconds

A similar experiment was conducted when the biotin solution was the one being delayed. As shown in Fig. 2.13, three possible scenarios that describe the interaction behaviors are schematically drawn. The measurement result is shown in Fig. 2.14. After

the injection of the streptavidin, drain current increases in 400 seconds, which is owing to the arrival of streptavidin. The biotin was applied at  $t = 660$  seconds. A small but observable current increase occurs 220 seconds after biotin injection. The increase is believed to be the signal of biotin. The biotin may be detected by binding either with the cross linkers or with the streptavidin. At  $t=1370$  seconds, the biotin-streptavidin complexes are detected. The scenario corresponds to the case described in Fig. 2.13(c). Since the concentration of the biotin solution ( $0.4\text{mM}$ ) is much higher than that of the streptavidin solution ( $1.67\mu\text{M}$ ), biotin molecules will not be consumed. There must be a third signal observed.

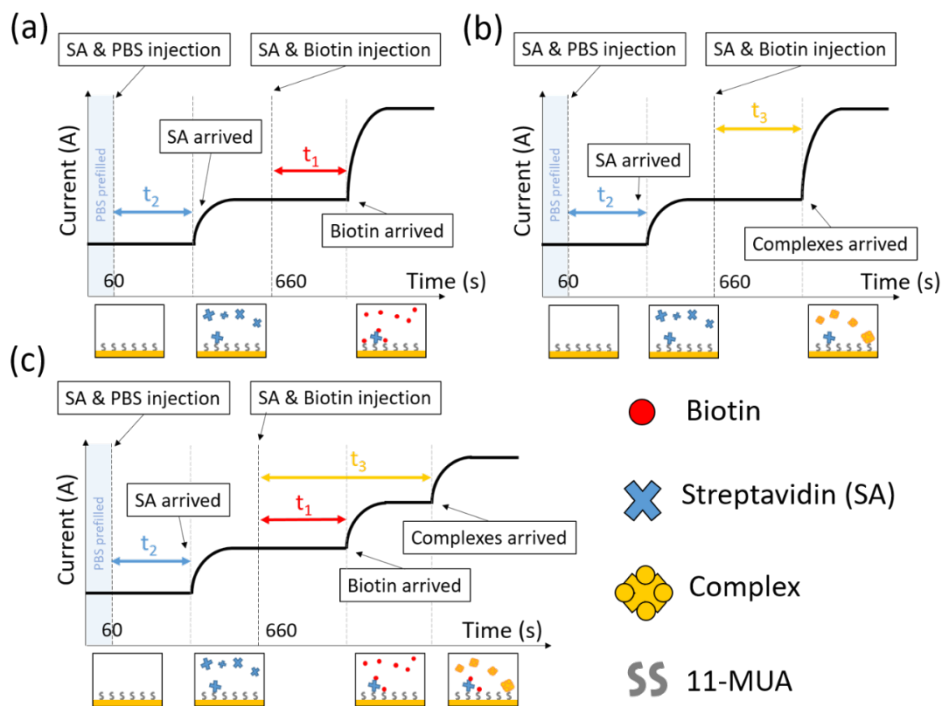


Fig. 2.13 Illustration of the current response scenarios for the biotin delay experiment

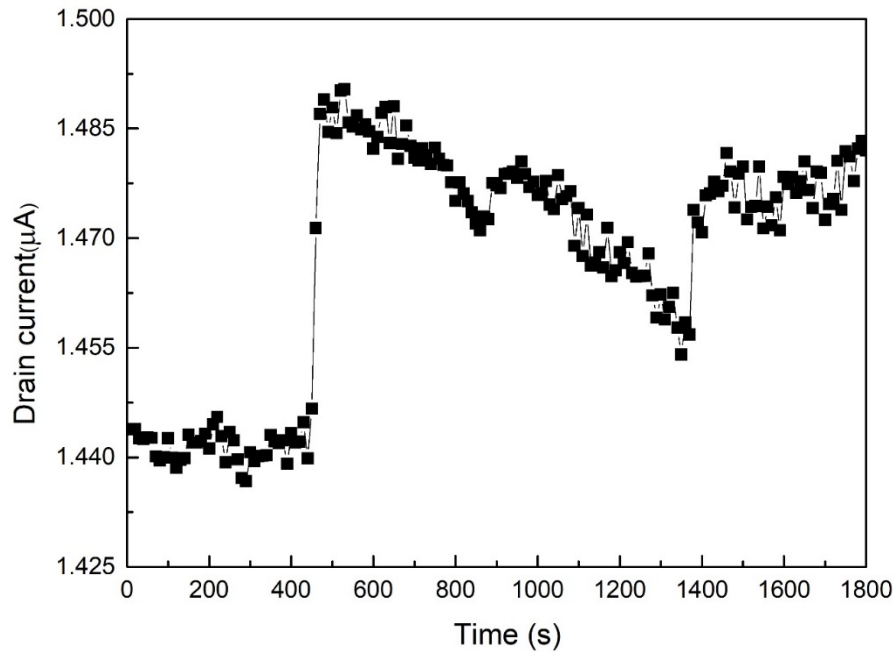


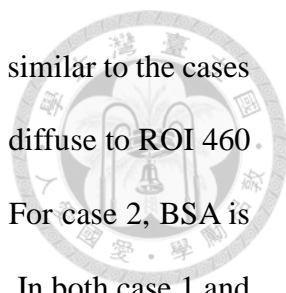
Fig. 2.14 Drain current response of the biotin delay experiment. PBS, streptavidin and biotin were introduced at  $t = 0, 60$  and  $660$  seconds

### 2.3.5 BSA control experiment

The specificity of the biotin-streptavidin biochemical reaction is next examined. For the biotin-streptavidin reaction, BSA is ideal as the reference group because of its non-specific property with streptavidin. In this study, in order to verify the specificity of the reaction in the microfluidic channel, biotin was replaced with BSA.

The diffusion behavior of BSA was first benchmarked. As shown in Fig. 2.15, an arrival time of 460 seconds is observed, which is regarded as the diffusion characteristic of BSA. Next, a delay experiment of BSA was conducted. After PBS prefilled at  $t=0$ , streptavidin and PBS were introduced into inlet 1 and inlet 2 at  $t=60$  seconds, respectively. The injection of PBS solution was replaced with BSA solution at 660 seconds.

Before the BSA delay experiment, several scenarios are considered. As streptavidin is introduced at the beginning, a diffusion time  $t_2$  of streptavidin molecules will be



observed. The injection of BSA will result in four possible conditions similar to the cases of biotin delay experiment as illustrated in Fig. 2.16. BSA molecules diffuse to ROI 460 seconds later. For case 1, BSA may be captured by the cross linkers. For case 2, BSA is captured by streptavidin at the ROI and form “non-specific” binding . In both case 1 and case 2, current increase will be observed when BSA reaches ROI, but case 2 is less likely. BSA should not bind with streptavidin. If non-specific binding complexes of BSA-streptavidin will be produced in the microfluidic channel, the drain current increase at a specific time, which is the signature of the complex, will be obtained. There is also a scenario that no binding between BSA and cross linkers or streptavidin when streptavidin is immobilized on the cross linkers. In such a case, only current response of streptavidin is seen.

The BSA delay measurement is shown in Fig. 2.17. Only one obvious current increment step 460 seconds after the injection of streptavidin is observed. The increase is attributed to the arrival of streptavidin. The entire transient response shows a stable current level after the drain current increase. The result clearly shows no BSA and BSA-streptavidin complexes are detected by our TFT sensor system. High specificity of the streptavidin-biotin reaction is indicated in the control BSA delay experiment. Our TFT biosensor provides a platform for analyzing protein-ligand biochemical reactions.

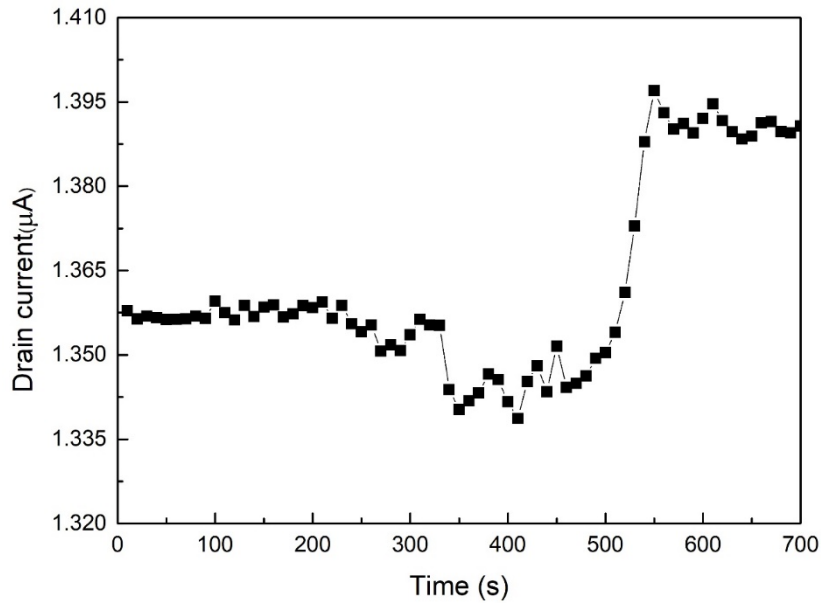


Fig. 2.15 Transient response of drain current with PBS pre-filled at  $t=0$  and  $0.4\text{mM}$  BSA injected at  $t=60$  seconds

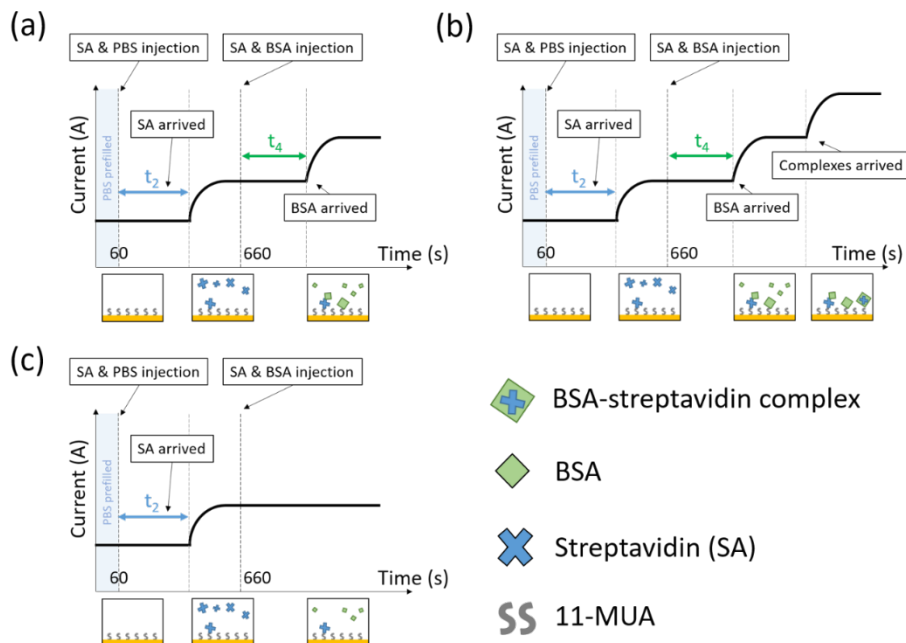


Fig. 2.16 Scenarios of possible BSA-streptavidin interactions once the analytes reach ROI

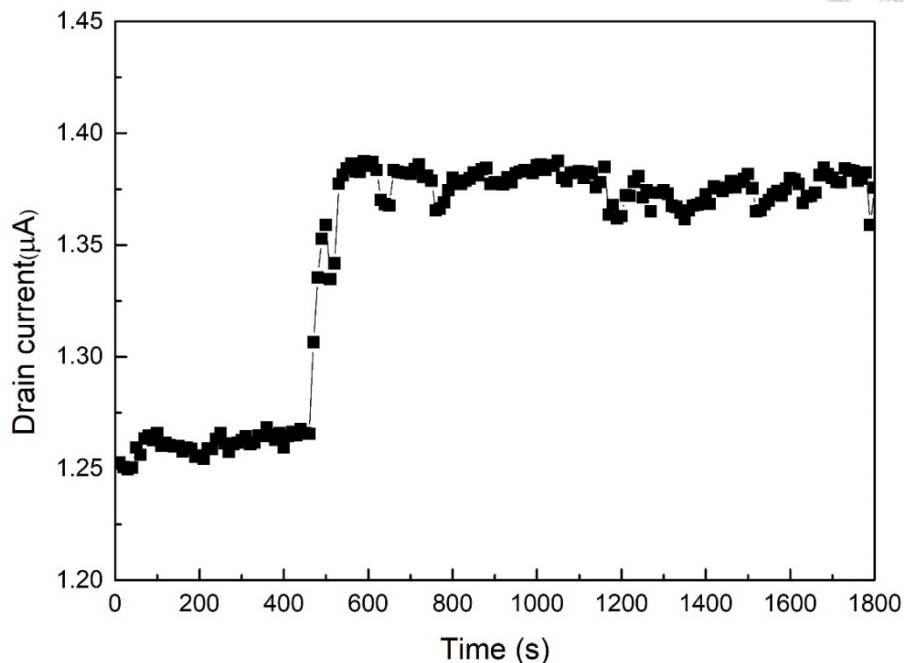


Fig. 2.17 Current response of BSA delay experiment. Streptavidin solution was introduced in inlet 1 at  $t=60$  s, and BSA solution was introduced in inlet 2 at  $t=660$ s

## 2.4 Summary

In this chapter, an IGZO TFT biosensor integrated with a Y-type external microfluidic channel chip is demonstrated. The device is designed for evaluating the mixing reaction situation of biomaterials. Biotin-streptavidin reaction is chosen to be detected and analyzed. First, the single biomaterial experiments are discussed. The diffusion time of the single biomaterials, i.e. biotin, streptavidin, BSA, are determined. The diffusion times are defined as the duration between the injection time and arrival time of these biomaterials. Next, time difference assumptions and experiments of the mixing reaction conditions are investigated and discussed. To further understand the reaction property, the delay experiments are also demonstrated. Finally, BSA is chosen for a control experiment to verify the non-specific binding situation. With the analysis and experiment framework, biochemical reaction properties such as the diffusion times, the excess and exhaust conditions of the reactants, and the product formation are understood.

# Chapter 3 IGZO-TFT Biosensors for Investigation of Protein-Ligand Kinetics

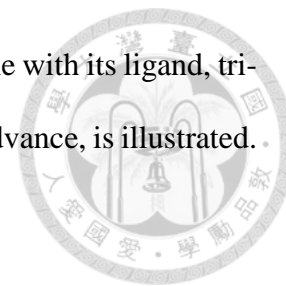


## 3.1 Introduction

### *Investigation of biochemical kinetics*

Recently, several methods exist for protein-ligand kinetics assessment. Classified by working principles, label-based measurement and label-free measurement are two categories for biosensors. Label-based detection, such as fluorescent cAMP analog [36], requires labeling molecules with fluorescence. Though the label-based methods have lower detection limit, the labeling process is complex and difficult [37]. As for label-free detection, such as surface plasmon resonance (SPR) [5], mass spectrometric (MS) [38], nuclear magnetic resonance (NMR) [39], isothermal titration calorimetry (ITC) [40], and quartz crystal monitor (QCM) [41], it requires large sample quantities or beforehand surface immobilization. The conformational and translational/rotational entropies may be changed by the protein immobilization and even the fluorescent labeling, which results in the influence of kinetics evaluation. Transistor-based biosensors is applicable without labeling, and large sample quantities. It has the advantages of real-time sensing, simplicity, compactness, high-sensitivity, and cost-effectiveness [41]. The technique is also suitable for lab-on-a-chip because of the miniaturization property [42]. For the transistor-based biosensors, the amount of electrical charges carried by biomolecules attribute to the readout. The diffusion characteristics, molecular concentration, and binding kinetic parameters are derivable by integrating with microfluidic system. In this thesis, to the best of understanding, an original contribution is made to protein-ligand kinetics free-space analysis by thin-film transistor (TFT) biosensor. The applicability of

the TFT biosensor on measuring the dissociation constant of lysozyme with its ligand, tri-N-acetyl-D-glucosamine (NAG<sub>3</sub>), without immobilizing protein in advance, is illustrated.



## 3.2 Material and Methods

### 3.2.1 Introduction of lysozyme and tri-N-acetylglucosamine

A protein called hen egg-white lysozyme is the target protein in this chapter. Lysozyme is an enzyme which breaks down the bacterial cell walls to protect protein or nucleic acid [43]. Accordingly, extraction efficiency of protein and nucleic acid is improved. The enzyme acts by catalyzing the hydrolysis of 1,4-beta-linkages between *N*-acetylmuramic acid and *N*-acetyl-D-glucosamine residues in peptidoglycans and between the *N*-acetyl-D-glucosamine residues in chitodextrins. The molar mass of lysozyme is about 14.4 kDa.

*N*-acetyl-D-glucosamine (NAG) is a monosaccharide and it is an amide between glucosamine and acetic acid. The saccharide has a molecular formula of C<sub>8</sub>H<sub>15</sub>NO<sub>6</sub>, a molar mass of 221.21 g/mol, and it is significant in several biological systems. Tri-N-acetyl-D-glucosamine (NAG<sub>3</sub>) is its trimer. There is strong binding affinity and longer reaction time between lysozyme and NAG<sub>3</sub>. Therefore, in this thesis, two biomaterials are selected as the target analytes to investigate the protein-ligand binding kinetics. Among them, protein refers to hen egg-white lysozyme and ligand refers to NAG<sub>3</sub>.

The hen egg-white lysozyme and NAG<sub>3</sub> were purchased from Sigma-Aldrich (USA). Both lysozyme and NAG<sub>3</sub> were prepared and diluted in 0.01×phosphate buffered saline (PBS) solution (PH7.4).





### 3.2.2 Measurement and experiment flow

#### *Measurement*

In this chapter, the Y-type microfluidic channel is replaced with a linear shape microfluidic channel (with width, length, and height being 1, 1, and 14 mm, respectively). The experiment setup is shown in Fig. 3.1 The ROI was functionalized with 11-MUA cross linker for 2 hours at room temperature and washed by PBS. The analytes were introduced into the microfluidic channel by Chemyx Fusion 200 syringe pump at flow rate of 300 nl/min. The measurement started with prefilling 0.01×PBS (pH 7.4) in the microfluidic channel at  $t = 0$  s. The target solutions were injected into the channel at  $t = 200$  s. Throughout the experiment, the electrical characteristics were characterized by Agilent 4155C semiconductor parameter analyzer. The TFT was biased at gate-source voltage,  $V_{GS}$ , of 10 V, and drain-source voltage,  $V_{DS}$ , of 5 V. The drain currents were sampled every 10 seconds.

#### *Experiment flow*

The experiment steps were illustrated in Fig. 3.2 The whole measurement can be separated into the following steps. First, the drain current response of a TFT biosensor was monitored over a period of time with filling 0.01×PBS in the microfluidic channel (bare chip). Next, the microfluidic channel was injected with 0.01×PBS (pH 7.4) at the time we assume  $t = 0$ . The current response of the injection is monitored and compared with that of bare chip. The purpose of the above steps is to understand the stress behavior of the TFT device and meanwhile the perturbation from solution injection. Typically, for a TFT with amorphous channel material layer, a recoverable current degradation will be observed during electrical stress. To characterize the kinetics of biochemical reactions, the concentrations of biochemical species in the microfluidic channel of different reaction times were correlated to drain current responses. The real-time drain current responses

of lysozyme and NAG<sub>3</sub> diffusing in the microfluidic channel was first characterized. Following the characterization, lysozyme solutions of different concentrations (5 mM, 1 mM, 0.5 mM, 0.1 mM) were introduced into the microfluidic channel to construct the correlation between the lysozyme concentration and the amount of the drain current variation induced by lysozyme molecules. In the second part, the lysozyme-NAG<sub>3</sub> binding kinetics were further investigated by characterizing the diffusion time and current increments of the molecules in the channel. The solutions of lysozyme and NAG<sub>3</sub> under various mixing ratios for different periods of reaction time were monitored by the TFT. Because lysozyme and NAG<sub>3</sub> bonded to the cross-linkers may block some binding sites of the complex (a phenomenon called screening effect in this work), the amount of current response of lysozyme and mixed solution may not directly reflect the actual concentration obtained from the calibration steps. The relationship of lysozyme concentration and drain current response was recalibrated. Based on the calibrated relationship, the amount of lysozyme concentration remained after reaction time is obtained. The details of calibration and fitting will be explained later. The association rate constant,  $k_a$ , and the dissociation constant,  $K_d$ , of the lysozyme-NAG<sub>3</sub> binding reaction can thus be obtained with the knowledge of the remained concentration of lysozyme.

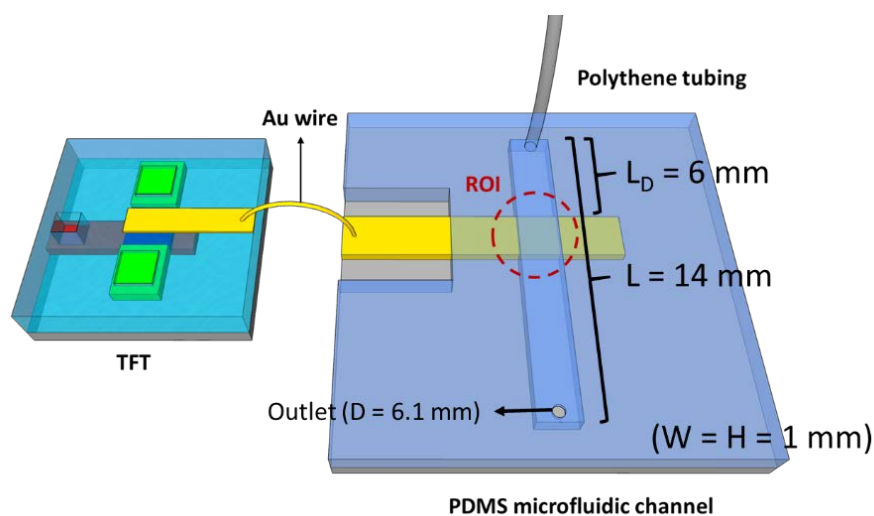


Fig. 3.1 Schematic of the IGZO-TFT biosensor with a linear-shaped microfluidic channel.

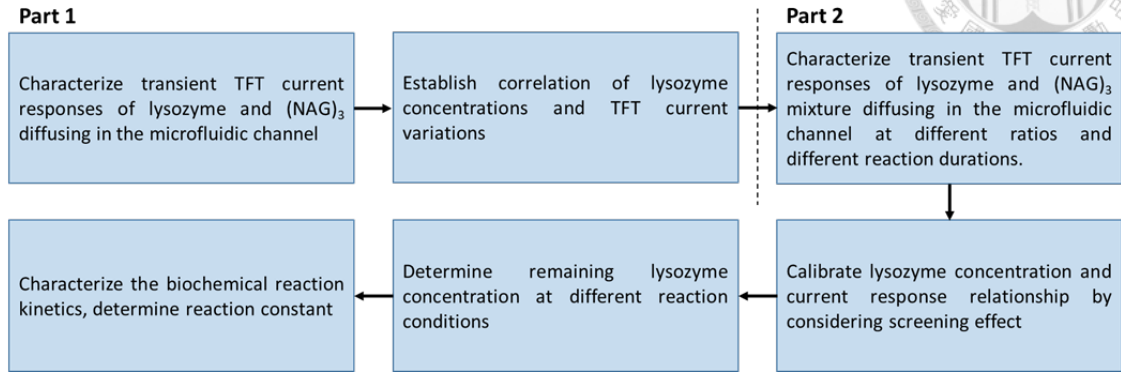


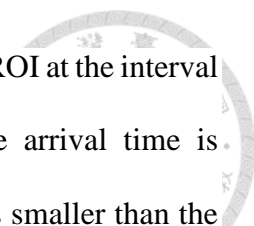
Fig. 3.2 Experimental flow which consists of two parts.

### 3.3 Results and Discussions

#### 3.3.1 Real-time analysis of lysozyme and tri-N-acetylglucosamine

The bare chip TFT current response with the microfluidic channel filled with PBS is demonstrated in Fig. 3.3. Because of the unavoidable defects in the IGZO channel, gate dielectric and thin film inter-faces, the amorphous type IGZO TFT under continuous electrical stress experiences a recoverable decrement of drain current [44]. The current decay may also be attributed to the ionic redistribution in solution [45]. It can also be affected by the solution injection turbulence in the microfluidic channel. When we injected  $0.01 \times \text{PBS}$  buffer to the inlet of the fluidic channel at  $t = 200$  s, a sudden increase of drain current at  $t = 300 \sim 350$  s was observed, which is the time of the solution diffusing to the sensing pad. The drain current will then resume to the stable state (see Fig. 3.4).

Next, the drain current increments of lysozyme with the concentration of 5, 1, 0.5, and 0.1mM were extracted. The transient current response of each concentration is shown in Fig. 3.5. Other than an injection turbulence as explained in the previous paragraph, the



curves experience the change of slope when the lysozyme arrives at the ROI at the interval between 500 and 540 s. Our previous work [46] suggests that the arrival time is independent of the concentration when the concentration is 1000 times smaller than the typical virial coefficient. Because lysozyme biomolecules carry positive charges under pH 7.4 [47], a decrease of drain current is observed. The amount of current decrease is directly correlated to the concentration of the lysozyme concentration. In Fig. 3.4, the change of drain current is determined by the starting and ending points, which the slope at the point of interest is becoming 70% higher or lower than the average current slope of 20 previous points in the time domain between, for example,  $t = 500$  and  $700$  s because most of lysozyme molecules arrive in the duration. The average is to eliminate the affect of sudden noise. The drain current change is the difference between the drain currents of starting point and ending point. Once most of the cross linkers have captured the lysozyme molecules arrived at ROI and thus the amount of drain current change is saturated, the drain current will gradually resume to the original path of current decrease. The phenomenon is generally valid for all of the single molecular solutions because electrical carriers in the TFT material structure will compensate charge variations in the accumulation type transistors, when the external perturbation becomes stable [48]. Finally, we plot the current change vs. lysozyme concentration (see Fig. 3.6) in logarithmic scale. A linearity  $R^2$  of 0.979 is obtained with a fitting curve shown in the figure.

We also conducted experiment on monitoring current changes of NAG<sub>3</sub> solution, but no obvious current change was observed. It suggests that NAG<sub>3</sub> solution doesn't carry net electrical charges in our experiment.

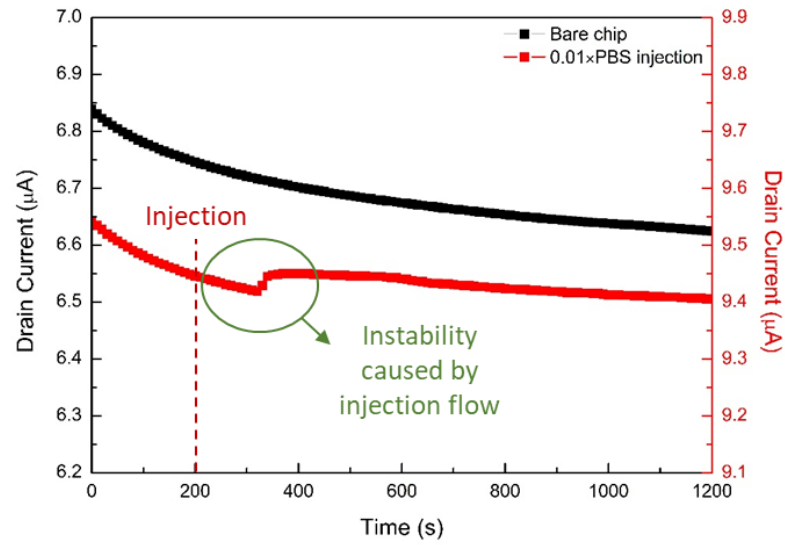


Fig. 3.3 Transient drain current properties of a bare TFT chip without and with the injection 0.01xPBS solution.

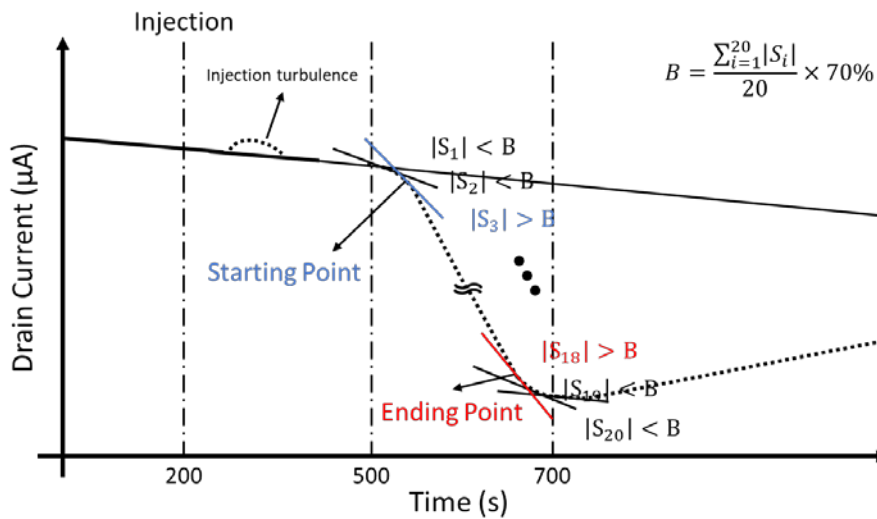


Fig. 3.4 A schematic drain current profile that illustrates physical events during biomaterial diffusion in the microfluidic channel. When the solution is injected at  $t=200$  s, we first observe injection turbulence. A decrease or increase (depending on species in the solution) of drain current indicates capture of biomaterials by the cross linkers in the ROI. The current change is determined by the slope changes, as compared with the

average of slopes of 20 points of earlier time.

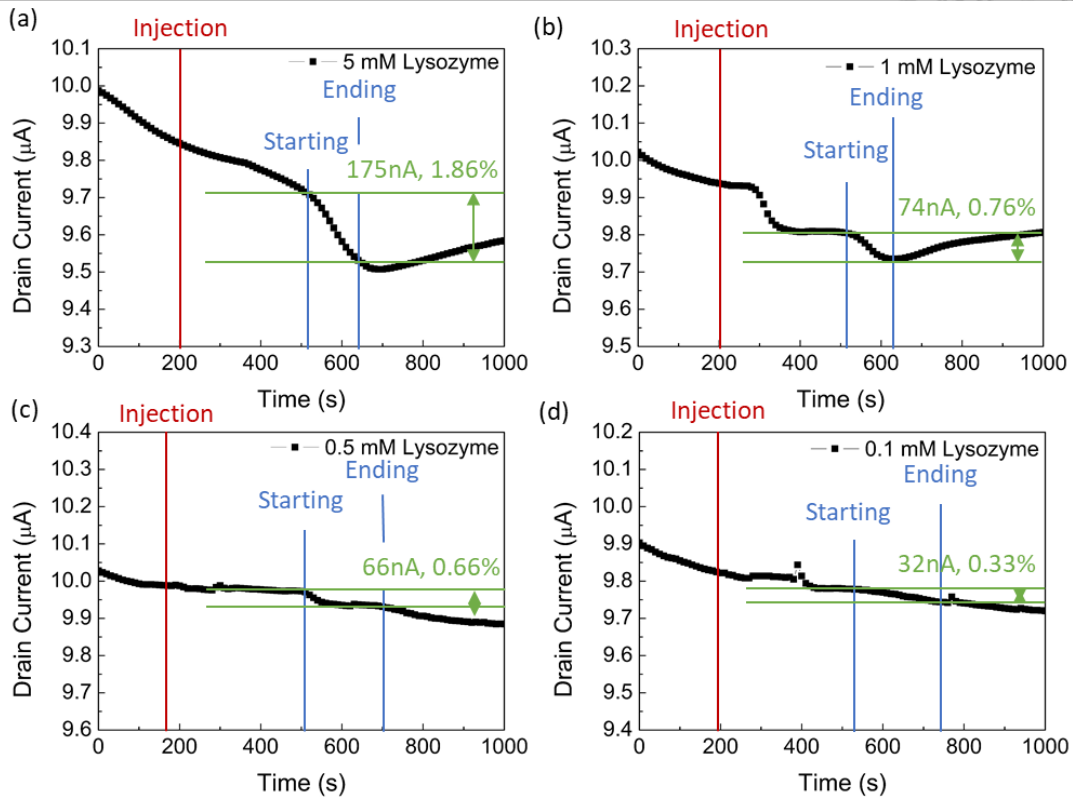


Fig. 3.5 Transient drain currents for lysozyme solutions of different concentrations.

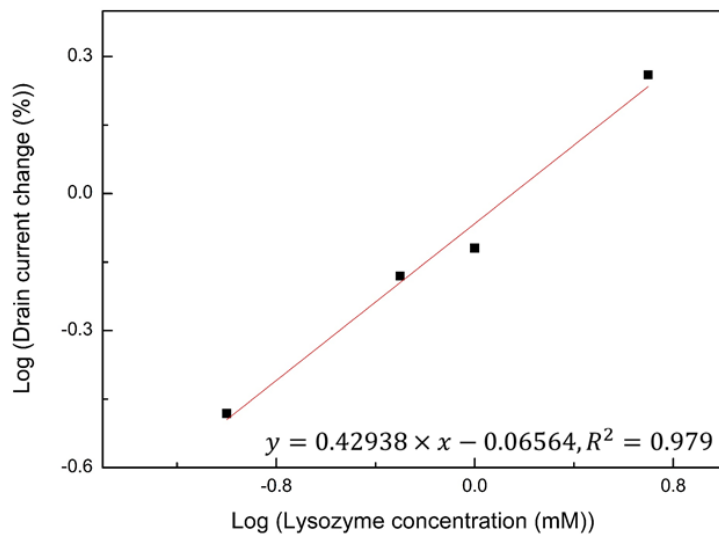
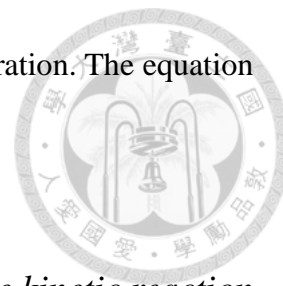


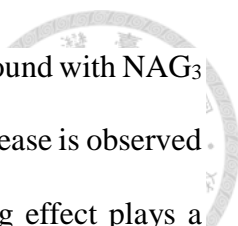
Fig. 3.6 Correlation of drain current change and lysozyme concentration. The equation of the fitting curve is shown in the plot.



### 3.3.2 Detection of lysozyme and tri-N-acetylglucosamine kinetic reaction

The reagent concentration of the biochemical reaction between lysozyme and NAG<sub>3</sub> is next analyzed. We prepared three different ratios of lysozyme and NAG<sub>3</sub> concentration, i.e., 1 mM lysozyme and 2.5 mM NAG<sub>3</sub>, 2.5 mM lysozyme and 2.5 mM NAG<sub>3</sub>, and 2.5 mM lysozyme and 1 mM NAG<sub>3</sub>. They were premixed in separate micro-centrifuges for 5 mins, 0.5, 1, 1.5, 2, 3, and 4 hrs before applying to the microfluidic channel. The transient drain current responses from, for example, the 1.5 hr-premix solution is shown in Fig. 3.7. The curve possesses basically two upward turning points that indicates signals of the reagents and products, one at around  $t = 500$  s while the other one at around 850 s. The first suggests the arrival lysozyme molecules at ROI, while the second is signals lysozyme-NAG<sub>3</sub> complex because the diffusion coefficient of the complex is smaller than that of lysozyme.[49]

As indicated earlier, though NAG<sub>3</sub> has insignificant effect of inducing additional electrical carriers, the smaller molecular weight of NAG<sub>3</sub> has higher diffusion coefficient and thus it reaches ROI before lysozyme and complex. NAG<sub>3</sub> is the first to bind with the cross linkers, causing the screening effect (see the illustration in Fig. 3.8). As a result, unlike the experiment with only lysozyme molecules in the solution that bind directly to the cross linkers, lysozyme in the mixture will face the situation that most of the binding sites in the cross linkers are occupied by NAG<sub>3</sub>. Drain current response profiles will be very different from solutions with solely lysozyme. The phenomenon, called screening effect in this work, is illustrated in Fig. 3.8. One should also note that in Fig. 3.4, drain



current decreases when lysozyme reaches ROI. However, the lysozyme bound with NAG<sub>3</sub> in Fig. 3.7 results in the increase of drain current. The trend of current increase is observed for all of the solutions with various mixing ratios, suggesting screening effect plays a critical role.

A method to calibrate out the screening effect is by compare the responses of short and long reaction time of the mixture. In our case, the reaction time of 5 mins is assumed to be too short for the reaction to happen, and is considered as “the initial point”. For example, for the mixture with 1 mM lysozyme and 2.5 mM NAG<sub>3</sub>, we assume the lysozyme concentration remains 1 mM after 5 mins of reaction (the duration can be shorter depending the analytes of the experiment). However, as shown in Fig. 3.7, current variations of 1 mM in the mixture is much smaller than the pure lysozyme solution. Ratio of the current change between mixture and pure solution of lysozyme is regarded as the revision factor and will be used to correlate lysozyme in the mixture and the fitting curve in Fig. 3.6. Table 1 shows the revision factors of different mixture solutions. As a result, the lysozyme current response in the mixture is multiplied by the revision factor. The modified current response is used to extract the lysozyme concentration remained in the solution following the fitting curve in Fig. 3.6.

The procedure of obtaining remained lysozyme concentration in Fig. 3.7 is elucidated as follows: for Fig. 3.7(a), lysozyme current increase is 0.20% for 1mM lysozyme and 2.5mM NAG<sub>3</sub>. From Table 1, 0.20% is multiplied by 2.21 to be 0.44%. Following the equation in Fig. 3.6, 0.44% of drain current change translates to 0.204 mM of lysozyme. The direct drain current change with different reaction times and the revised response of three mixture solutions is shown in Fig. 3.9.



The remained lysozyme concentrations at various reaction times of three mixtures are shown in Fig. 3.10, along with the fitting curves and equations.

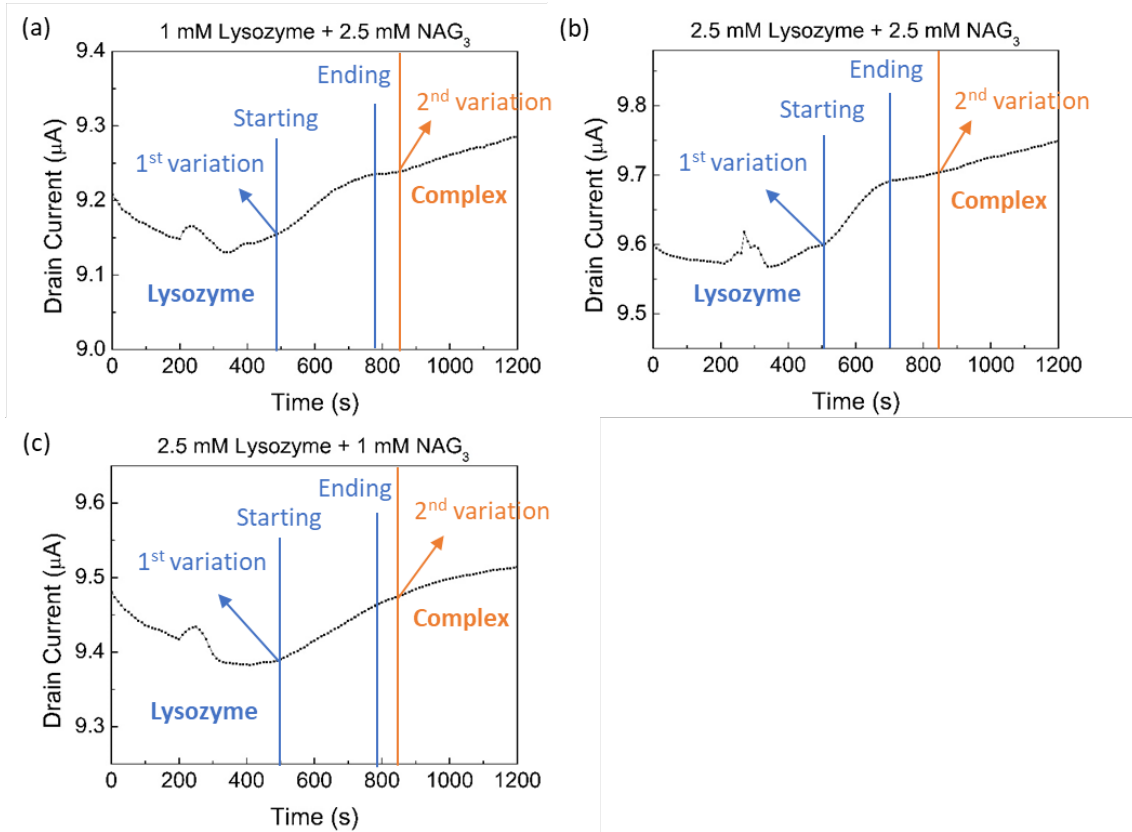


Fig. 3.7 Transient TFT drain currents for mixtures of (a) 1 mM lysozyme and 2.5 mM NAG<sub>3</sub>, (b) 2.5 mM lysozyme and 2.5 mM NAG<sub>3</sub>, and (c) 2.5 mM lysozyme and 1 mM NAG<sub>3</sub>. They were all reacted for 1.5 hrs before dispersing to the inlet of microfluidic channel. There are two upward turning points in the curves, one at around 500s and the other at around 850s. The first one corresponds to the arrival of lysozyme while the second of lysozyme-NAG<sub>3</sub> complex.

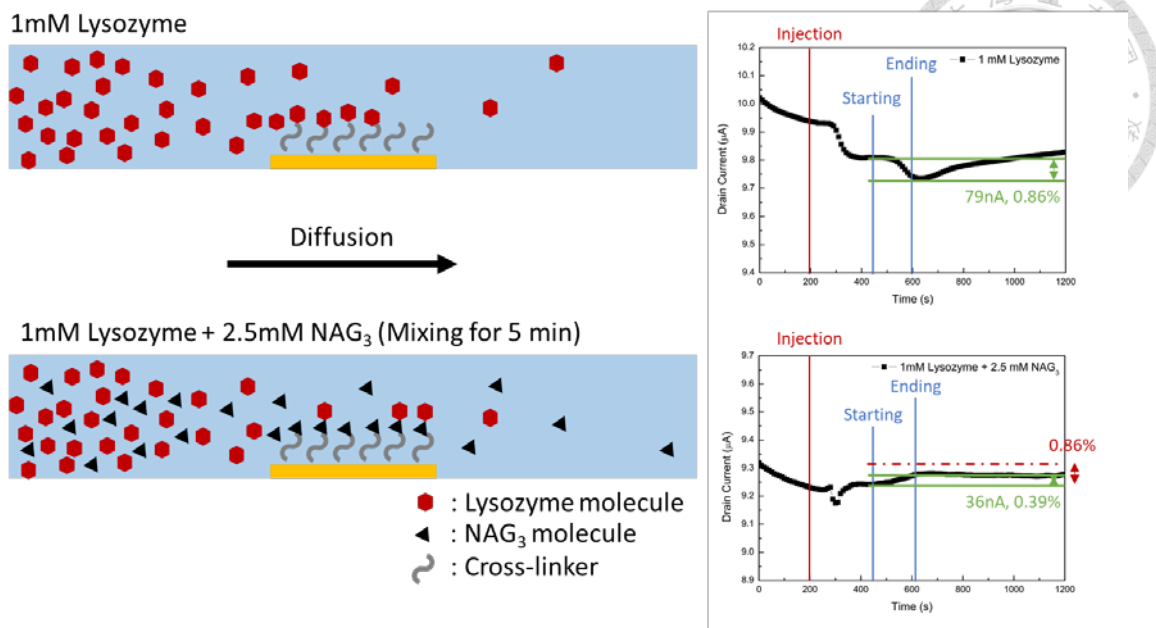


Fig. 3.8 Illustration of molecule capture process of (a) Lysozyme solution (b) lysozyme + NAG<sub>3</sub> solution. The induced drain currents are shown in the right. Note that in addition to the screening effect, with the presence of NAG<sub>3</sub>, the drain current will be increased instead of decreased as opposed to the case of pure lysozyme solution.

Table 2. Revision Factors of the Mixtures in Our Experiment

Mixing Ratio	Initial Lysozyme Concentration (mM)	Raw Current Response (%)	Current Response <sup>**</sup> (%)	Revision Factor
1:2.5	1	0.39	0.86	2.21
2.5:2.5	2.5	0.52	1.27	2.44
2.5:1	2.5	0.86	1.27	1.48

<sup>\*\*</sup> Based on the correlation in Fig. 3.6.

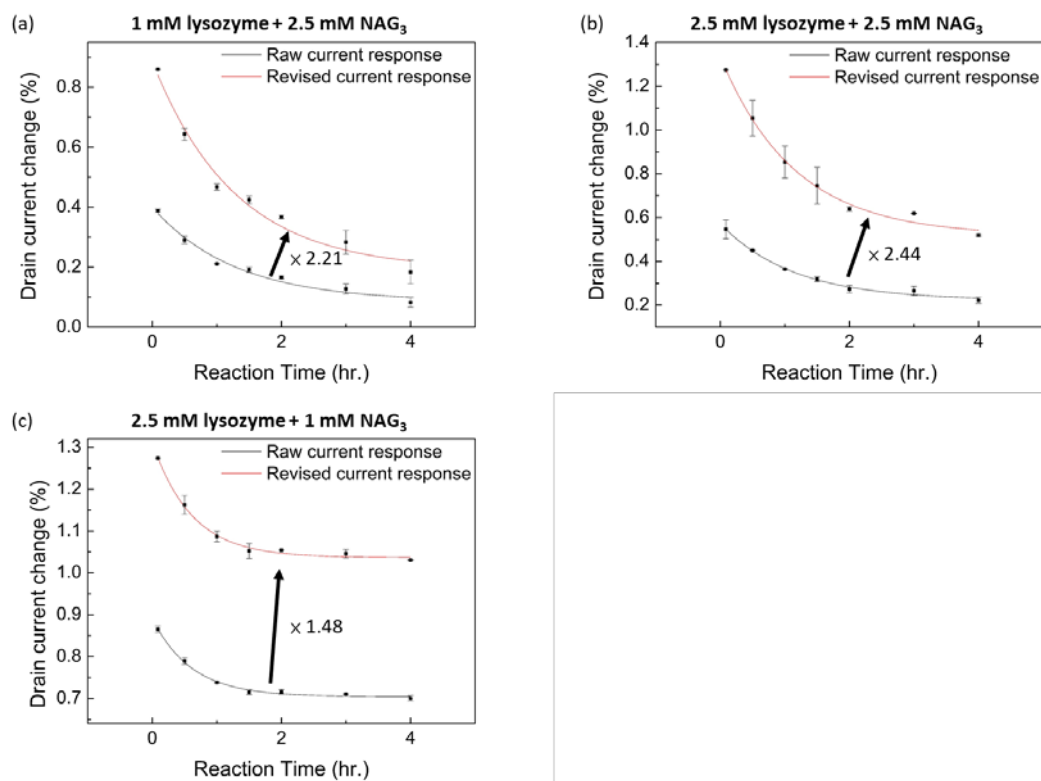


Fig. 3.9 Drain current changes of the raw and revised responses at different reaction times.

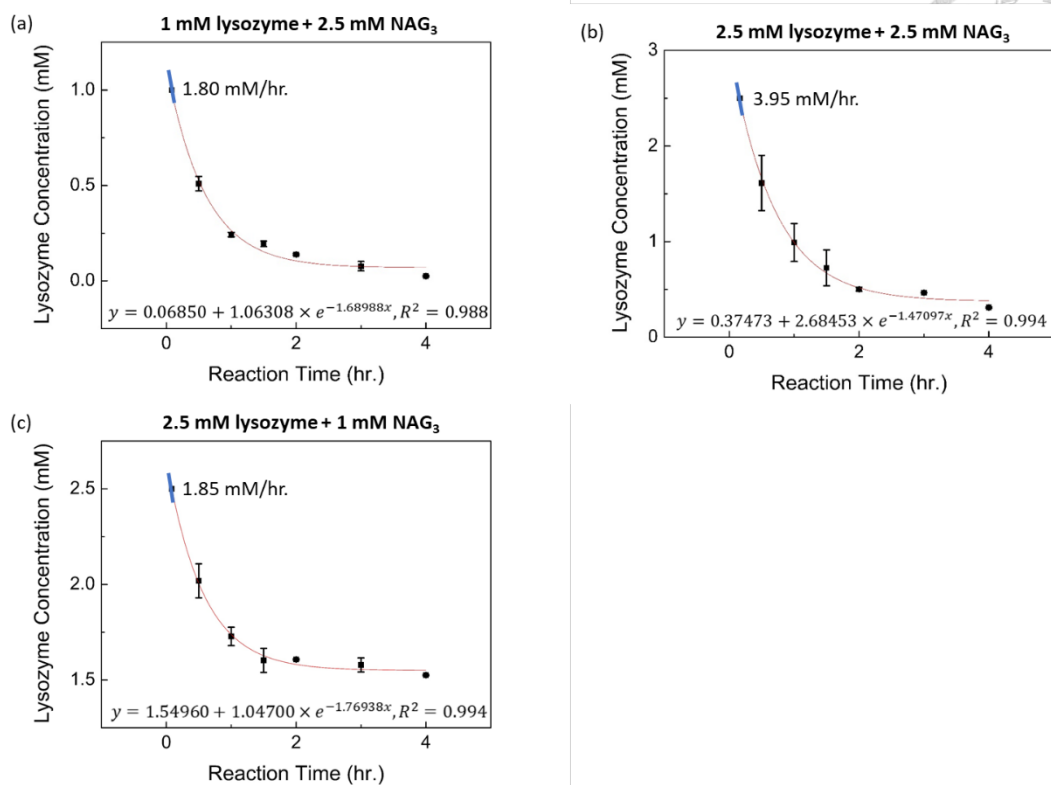


Fig. 3.10 Correlation between the remained lysozyme concentration and the reaction time for (a) 1 mM lysozyme and 2.5 mM NAG<sub>3</sub>, (b) 2.5 mM lysozyme and 2.5 mM NAG<sub>3</sub>, and (c) 2.5 mM lysozyme and 1 mM NAG<sub>3</sub> mixing solutions.

### 3.3.3 Biochemical constants analysis

#### *Association rate constant*

By taking the derivative of the equations at  $x = 0$  ( $x$  is the reaction time), the initial reaction rates can be obtained and are labelled in the Fig. 3.10.

Alternatively, the reaction rate can be written as:

$$\text{Reaction rate} = k_a[\text{Lysozyme}]^a[\text{NAG}_3]^b \quad (1)$$

, where  $k_a$  represents the association rate constant,  $a$  and  $b$  are the partial orders. At  $t=0$ ,



(1) is expressed as,

$$1.80 \left(\frac{mM}{hr.}\right) = k_a [1]^a [2.5]^b \quad (2)$$

$$3.95 \left(\frac{mM}{hr.}\right) = k_a [2.5]^a [2.5]^b \quad (3)$$

$$1.85 \left(\frac{mM}{hr.}\right) = k_a [2.5]^a [1]^b \quad (4)$$

(2), (3) and (4) are the reaction rates corresponding to figure 9(a), (b) and (c), respectively.

By solving equations 2-4, the calculation results, which are calculated from the experiment results and reflect the real reaction situation, are 0.86 and 0.83 for a and b and the association rate constants,  $k_a$ , is  $0.841 \text{ mM}^{-1}\text{hr}^{-1}$  ( $0.234 \text{ M}^{-1}\text{s}^{-1}$ ).

Because the lysozyme-NAG<sub>3</sub> binding reaction is an elementary reaction, the partial orders a and b obtained above are correlated to the stoichiometric coefficients [50]. The reaction formula is written as:



Ideally, both the stoichiometric coefficients of lysozyme and NAG<sub>3</sub> are 1. Thus, both the partial orders, a, and b, should be 1. The values we obtained from the experiment suggest the deviation of lysozyme and NAG<sub>3</sub> bioreaction from the ideal case.

#### *Dissociation constant*

The lysozyme-NAG<sub>3</sub> binding reaction is assumed to reach the equilibrium state after 4 hrs. According to Fig. 3.10, the remained lysozyme concentrations after 4 hrs. of reaction are 0.025, 0.311, and 1.523 mM for mixing ratio of 1:2.5, 2.5:2.5, and 2.5:1, respectively. The dissociation constant,  $K_d$ , can be estimated to be:

$$K_d = \frac{[\text{Lysozyme}][\text{NAG}_3]}{[\text{Complex}]} \quad (5)$$

Based on the reaction formula (5) and equation (6), the dissociation constants of three mixing solutions are shown in Table 2.

It is worth mentioning that the dissociation constant obtained from Fig. 3.10(b) (2.5

mM lysozyme and 2.5 mM NAG<sub>3</sub>) is deviated from the rest two. Also, the instantaneous reaction rate, by taking the derivative of the equation inserted in Fig. 3.10(b) at  $x = 4$ , for sample of 2.5:2.5 mixing ratio is 0.011 mM/hr., which is much higher than 0.002 mM/hr. for samples of mixing ratios of both 1:2.5 and 2.5:1. The higher value of the instantaneous reaction rate means the 2.5:2.5 solution hasn't reached equilibrium state even after 4 hrs of reaction. On the other hand, the values obtained from 1:2.5 and 2.5:1 mixtures are close to those reported in the literature using other approaches (see Table 3).

The parameters explored in this work, such as association rate constant and dissociation constant, are key to the investigation of biochemical reactions, especially for drug discovery. They help researchers to understand the efficacy and safety of drugs. The IGZO-TFT biosensor as proposed in this work provides efficient monitoring of biochemical reactions. Our approach doesn't require labeling or forehanded immobilization of target protein on the sensing surface, thus avoiding potential misleading results in some conventional methods [17, 51]. The partial order as obtained from rate equations help to understand stoichiometry of the protein-ligand reaction. In addition, the TFT and microfluidic channel can be fabricated in array, a parallel approach to detect biochemical reactions, so that high-throughput measurement for drug industry can be realized.

Table 3. Remained Lysozyme, NAG<sub>3</sub> and Complex Concentrations of Three Mixtures, and the Calculated Results of Dissociation Constant,  $K_d$

Ratio	[Lysozyme] (mM)	[NAG <sub>3</sub> ] (mM)	[Complex] (mM)	$K_d$ ( $\mu$ M)
1:2.5	0.025	1.525	0.975	39.10
2.5:2.5	0.311	0.311	2.189	43.88

2.5:1

1.523

0.026

0.974

39.10



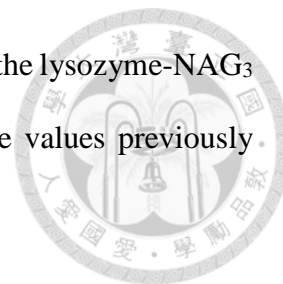
Table 4. Comparisons of Dissociation Constant,  $K_d$ , of Lysozyme–NAG<sub>3</sub> Based on Our Approach and Others Reported in the Literature

Method	$K_d$ ( $\mu\text{M}$ )	Reference
Electrospray Ionization Mass Spectrometry	19	[52]
Transient Induced Molecular Electronic Spectroscopy	39.81	[17]
Nanoelectrospray Ionization Mass Spectrometry	39	[53]
This Work	39.10	

### 3.4 Summary

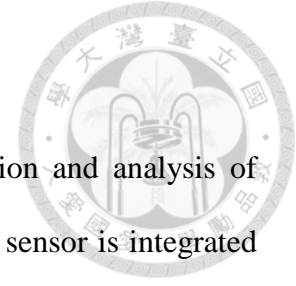
In this chapter, the reaction kinetics are further analyzed by our TFT biosensor. The correlation between the current response and lysozyme concentration was constructed. Based on the relation, the observed current response induced by lysozyme molecules were calibrated through the revision process and the conversion of revised response into remained lysozyme concentration was conducted. The reaction reacts quickly at first and gradually reaches the equilibrium state as the time went by. In addition, the initial reaction rates and lysozyme equilibrium concentrations were extracted from the remained lysozyme versus reaction time fitting curves. The parameters led to the calculation of

partial orders, association rate constant, and dissociation constant for the lysozyme-NAG<sub>3</sub> binding reaction. The resulting dissociation constant is close to the values previously reported in other works.





## Chapter 4 Conclusions



An IGZO-TFT biosensor is a robust platform for the detection and analysis of biochemical reaction or the pharmaceutical application because the sensor is integrated with numerous kinds of tailored microfluidic channels. In this work, for two experiment purposes, two kinds of microfluidic channels were applied, Y-type and linear shape.

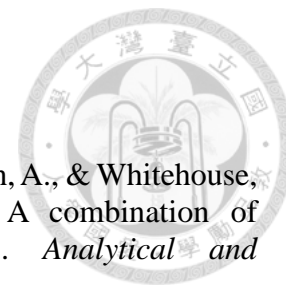
In chapter 2, a Y-type microfluidic channel was integrated with the TFT biosensor as a micro-mixer. Biotin and streptavidin, as target reactants, were introduced into the channel separately to benchmark the diffusion times. After the diffusion properties confirmation, both the reactants were injected at two separate inlets simultaneously. The exhaust of streptavidin and product formation were realized by the diffusion times. To further understand the biotin and streptavidin biochemical reaction, the delay experiments were conducted. The experiment results coincided with the previous set of measurement. Furthermore, the specificity of biotin-streptavidin biochemical reaction was examined through injecting BSA, which is nonspecific to streptavidin.

In chapter 3, a linear shape microfluidic channel provided a platform for monitoring protein-ligand binding kinetics. In this case, lysozyme and its ligand, tri-N-acetylglucosamine (NAG<sub>3</sub>), were applied. Before the kinetic analysis, the drain current response versus lysozyme concentration relation was acquired. The lysozyme-NAG<sub>3</sub> binding reaction took place in the micro-centrifuge under several mixing ratios for different reaction times. The lysozyme drain current responses for the mixtures were extracted and converted by the drain current response versus lysozyme concentration relation into remained lysozyme concentrations after response calibration, which was in response to the screening effect. Based on the correlation between the remained lysozyme concentration and the reaction time, the kinetic parameters, such as partial orders, the

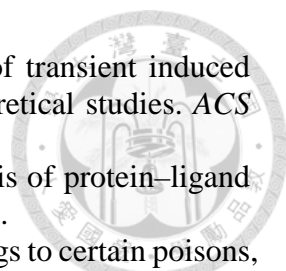
association rate constant, and the dissociation constant, were derivable.

The label-free and no requirement of forehanded protein immobilization, which may mislead the results of kinetic parameters, low sample consumption and low-cost properties make the IGZO-TFT biosensor an ideal candidate for the biochemical investigation. With proper design of the microfluidic channel, the biosensor is also applicable for drug discovery because of the high-throughput property.

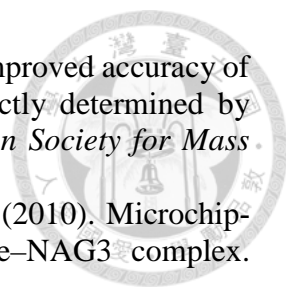
## REFERENCE



- [1] Lindholm-Sethson, B., Nyström, J., Geladi, P., Koeppel, R., Nelson, A., & Whitehouse, C. (2003). Are biosensor arrays in one membrane possible? A combination of multifrequency impedance measurements and chemometrics. *Analytical and bioanalytical chemistry*, 377(3), 478-485.
- [2] Subrahmanyam, S., Piletsky, S. A., & Turner, A. P. (2002). Application of natural receptors in sensors and assays. *Analytical chemistry*, 74(16), 3942-3951.
- [3] Rasooly, A., & Jacobson, J. (2006). Development of biosensors for cancer clinical testing. *Biosensors and Bioelectronics*, 21(10), 1851-1858.
- [4] Mohanty, S. P., & Kougiyanos, E. (2006). Biosensors: a tutorial review. *Ieee Potentials*, 25(2), 35-40.
- [5] Patching, S. G. (2014). Surface plasmon resonance spectroscopy for characterisation of membrane protein–ligand interactions and its potential for drug discovery. *Biochimica et Biophysica Acta (BBA)-Biomembranes*, 1838(1), 43-55.
- [6] Garber, E. A. (2008). Detection of melamine using commercial enzyme-linked immunosorbent assay technology. *Journal of food protection*, 71(3), 590-594.
- [7] Kurien, B. T., & Scofield, R. H. (2015). Western blotting: an introduction. In *Western Blotting* (pp. 17-30): Springer.
- [8] Cheng, S., Hideshima, S., Kuroiwa, S., Nakanishi, T., & Osaka, T. (2015). Label-free detection of tumor markers using field effect transistor (FET)-based biosensors for lung cancer diagnosis. *Sensors and Actuators B: Chemical*, 212, 329-334.
- [9] Yakimova, R., Steinhoff, G., Petoral Jr, R., Vahlberg, C., Khranovskyy, V., Yazdi, G., . . . Spetz, A. L. (2007). Novel material concepts of transducers for chemical and biosensors. *Biosensors and Bioelectronics*, 22(12), 2780-2785.
- [10] Lin, J.-C., Huang, B.-R., & Yang, Y.-K. (2013). IGZO nanoparticle-modified silicon nanowires as extended-gate field-effect transistor pH sensors. *Sensors and Actuators B: Chemical*, 184, 27-32.
- [11] Liu, X., Lin, P., Yan, X., Kang, Z., Zhao, Y., Lei, Y., . . . Zhang, Y. (2013). Enzyme-coated single ZnO nanowire FET biosensor for detection of uric acid. *Sensors and Actuators B: Chemical*, 176, 22-27.
- [12] Guo, D., Zhuo, M., Zhang, X., Xu, C., Jiang, J., Gao, F., . . . Wang, T. (2013). Indium-tin-oxide thin film transistor biosensors for label-free detection of avian influenza virus H5N1. *Analytica chimica acta*, 773, 83-88.
- [13] Reyes, P. I., Ku, C.-J., Duan, Z., Lu, Y., Solanki, A., & Lee, K.-B. (2011). ZnO thin film transistor immunosensor with high sensitivity and selectivity. *Applied Physics Letters*, 98(17), 173702.
- [14] Jung, J., Kim, S. J., Yoon, D. H., Kim, B., Park, S. H., & Kim, H. J. (2012). Electrical responses of artificial DNA nanostructures on solution-processed In-Ga-Zn-O thin-film transistors with multistacked active layers. *ACS applied materials & interfaces*, 5(1), 98-102.
- [15] Kim, S. J., Jung, J., Yoon, D. H., & Kim, H. J. (2012). The effect of various solvents on the back channel of solution-processed In–Ga–Zn–O thin-film transistors intended for biosensor applications. *Journal of Physics D: Applied Physics*, 46(3), 035102.
- [16] Ruess, J., Miliás-Argeitis, A., & Lygeros, J. (2013). Designing experiments to understand the variability in biochemical reaction networks. *Journal of the Royal Society Interface*, 10(88), 20130588.
- [17] Zhang, T., Wei, T., Han, Y., Ma, H., Samieegohar, M., Chen, P.-W., . . . Lo, Y.-H.

- 
- (2016). Protein–ligand interaction detection with a novel method of transient induced molecular electronic spectroscopy (TIMES): experimental and theoretical studies. *ACS central science*, 2(11), 834-842.
- [18] Cala, O., Guillière, F., & Krimm, I. (2014). NMR-based analysis of protein–ligand interactions. *Analytical and bioanalytical chemistry*, 406(4), 943-956.
- [19] Langley, J. N. (1905). On the reaction of cells and of nerve-endings to certain poisons, chiefly as regards the reaction of striated muscle to nicotine and to curari. *The Journal of physiology*, 33(4-5), 374-413.
- [20] Swinney, D. C. (2009). The role of binding kinetics in therapeutically useful drug action. *Current opinion in drug discovery & development*, 12(1), 31-39.
- [21] Copeland, R. A., Pompliano, D. L., & Meek, T. D. (2006). Drug–target residence time and its implications for lead optimization. *Nature reviews Drug discovery*, 5(9), 730.
- [22] Pan, A. C., Borhani, D. W., Dror, R. O., & Shaw, D. E. (2013). Molecular determinants of drug–receptor binding kinetics. *Drug discovery today*, 18(13-14), 667-673.
- [23] Gobby, D., Angeli, P., & Gavriilidis, A. (2001). Mixing characteristics of T-type microfluidic mixers. *Journal of Micromechanics and microengineering*, 11(2), 126.
- [24] Lee, C.-Y., Chang, C.-L., Wang, Y.-N., & Fu, L.-M. (2011). Microfluidic mixing: a review. *International journal of molecular sciences*, 12(5), 3263-3287.
- [25] Riahi, R., Tamayol, A., Shaegh, S. A. M., Ghaemmaghami, A. M., Dokmeci, M. R., & Khademhosseini, A. (2015). Microfluidics for advanced drug delivery systems. *Current Opinion in Chemical Engineering*, 7, 101-112.
- [26] Teh, S.-Y., Lin, R., Hung, L.-H., & Lee, A. P. (2008). Droplet microfluidics. *Lab on a Chip*, 8(2), 198-220.
- [27] Yamada, M., Sugaya, S., Naganuma, Y., & Seki, M. (2012). Microfluidic synthesis of chemically and physically anisotropic hydrogel microfibers for guided cell growth and networking. *Soft Matter*, 8(11), 3122-3130.
- [28] Ahmed, D., Mao, X., Juluri, B. K., & Huang, T. J. (2009). A fast microfluidic mixer based on acoustically driven sidewall-trapped microbubbles. *Microfluidics and nanofluidics*, 7(5), 727.
- [29] Zhang, J., Tan, K., Hong, G., Yang, L., & Gong, H. (2001). Polymerization optimization of SU-8 photoresist and its applications in microfluidic systems and MEMS. *Journal of Micromechanics and microengineering*, 11(1), 20.
- [30] Kendall, C., Ionescu-Matiu, I., & Dreesman, G. R. (1983). Utilization of the biotin/avidin system to amplify the sensitivity of the enzyme-linked immunosorbent assay (ELISA). *Journal of immunological methods*, 56(3), 329-339.
- [31] VON BOXBERG, Y., WÜTZ, R., & SCHWARZ, U. (1990). Use of the biotin-avidin system for labelling, isolation and characterization of neural cell-surface proteins. *European journal of biochemistry*, 190(2), 249-256.
- [32] Savran, C., Burg, T., Fritz, J., & Manalis, S. (2003). Microfabricated mechanical biosensor with inherently differential readout. *Applied Physics Letters*, 83(8), 1659-1661.
- [33] Eteshola, E., & Leckband, D. (2001). Development and characterization of an ELISA assay in PDMS microfluidic channels. *Sensors and Actuators B: Chemical*, 72(2), 129-133.
- [34] Segato, T. P., Coltro, W. K. T., de Jesus Almeida, A. L., de Oliveira Piazzetta, M. H., Gobbi, A. L., Mazo, L. H., & Carrilho, E. (2010). A rapid and reliable bonding process for microchip electrophoresis fabricated in glass substrates. *Electrophoresis*, 31(15), 2526-2533.
- [35] Jo, M. C., & Guldiken, R. (2013). Dual surface acoustic wave-based active mixing

- in a microfluidic channel. *Sensors and Actuators A: Physical*, 196, 1-7.
- [36] Peuker, S., Cukkemane, A., Held, M., Noé, F., Kaupp, U. B., & Seifert, R. (2013). Kinetics of ligand-receptor interaction reveals an induced-fit mode of binding in a cyclic nucleotide-activated protein. *Biophysical journal*, 104(1), 63-74.
- [37] Huang, Y.-W., Wu, C.-S., Chuang, C.-K., Pang, S.-T., Pan, T.-M., Yang, Y.-S., & Ko, F.-H. (2013). Real-time and label-free detection of the prostate-specific antigen in human serum by a polycrystalline silicon nanowire field-effect transistor biosensor. *Analytical chemistry*, 85(16), 7912-7918.
- [38] Cong, Y., Katipamula, S., Trader, C. D., Orton, D. J., Geng, T., Baker, E. S., & Kelly, R. T. (2016). Mass spectrometry-based monitoring of millisecond protein–ligand binding dynamics using an automated microfluidic platform. *Lab on a Chip*, 16(9), 1544-1548.
- [39] Iešmantavičius, V., Dogan, J., Jemth, P., Teilum, K., & Kjaergaard, M. (2014). Helical propensity in an intrinsically disordered protein accelerates ligand binding. *Angewandte Chemie International Edition*, 53(6), 1548-1551.
- [40] Perspicace, S., Rufer, A. C., Thoma, R., Mueller, F., Hennig, M., Ceccarelli, S., . . . Seelig, J. (2013). Isothermal titration calorimetry with micelles: thermodynamics of inhibitor binding to carnitine palmitoyltransferase 2 membrane protein. *FEBS open bio*, 3(1), 204-211.
- [41] Duan, X., Li, Y., Rajan, N. K., Routenberg, D. A., Modis, Y., & Reed, M. A. (2012). Quantification of the affinities and kinetics of protein interactions using silicon nanowire biosensors. *Nature nanotechnology*, 7(6), 401.
- [42] Choi, K., Kim, J.-Y., Ahn, J.-H., Choi, J.-M., Im, M., & Choi, Y.-K. (2012). Integration of field effect transistor-based biosensors with a digital microfluidic device for a lab-on-a-chip application. *Lab on a Chip*, 12(8), 1533-1539.
- [43] Primo, E. D., Otero, L. H., Ruiz, F., Klinke, S., & Giordano, W. (2018). The disruptive effect of lysozyme on the bacterial cell wall explored by an in-silico structural outlook. *Biochemistry and Molecular Biology Education*, 46(1), 83-90.
- [44] Cho, I.-T., Lee, J.-M., Lee, J.-H., & Kwon, H.-I. (2008). Charge trapping and detrapping characteristics in amorphous InGaZnO TFTs under static and dynamic stresses. *Semiconductor Science and Technology*, 24(1), 015013.
- [45] Guzman, K. D., Karnik, R. N., Newman, J. S., & Majumdar, A. (2006). Spatially controlled microfluidics using low-voltage electrokinetics. *Journal of microelectromechanical systems*, 15(1), 237-245.
- [46] Chen, T.-Y., Yang, T.-H., Wu, N.-T., Chen, Y.-T., & Huang, J.-J. (2017). Transient analysis of streptavidin-biotin complex detection using an IGZO thin film transistor-based biosensor integrated with a microfluidic channel. *Sensors and Actuators B: Chemical*, 244, 642-648.
- [47] Shao, D., Xu, K., Song, X., Hu, J., Yang, W., & Wang, C. (2009). Effective adsorption and separation of lysozyme with PAA-modified Fe<sub>3</sub>O<sub>4</sub>@ silica core/shell microspheres. *Journal of colloid and interface science*, 336(2), 526-532.
- [48] Parker, G. (2001). *Encyclopedia of materials: science and technology* (2<sup>nd</sup> ed.); 299-304.
- [49] Clark, S. M., & Konermann, L. (2004). Screening for Noncovalent Ligand– Receptor Interactions by Electrospray Ionization Mass Spectrometry-Based Diffusion Measurements. *Analytical chemistry*, 76(5), 1257-1263.
- [50] College, O. (2015). *Chemistry*: Houston, Texas : OpenStax College, Rice University;
- [51] Bernetti, M., Cavalli, A., & Mollica, L. (2017). Protein–ligand (un) binding kinetics as a new paradigm for drug discovery at the crossroad between experiments and modelling. *MedChemComm*, 8(3), 534-550.

- 
- [52] Jaquillard, L., Saab, F., Schoentgen, F., & Cadene, M. (2012). Improved accuracy of low affinity protein–ligand equilibrium dissociation constants directly determined by electrospray ionization mass spectrometry. *Journal of The American Society for Mass Spectrometry*, 23(5), 908-922.
- [53] Svobodová, J., Mathur, S., Muck, A., Letzel, T., & Svatoš, A. (2010). Microchip-ESI-MS determination of dissociation constant of the lysozyme–NAG3 complex. *Electrophoresis*, 31(15), 2680-2685.